# Performance Analysis of a Spectrum Sharing System in the Modulation-based Dimension

Truc Thanh Tran, Duy H. N. Nguyen, Tuan Do-Hong, and Ngo Van Sy

***Abstract*—This paper studies the exploitation of the modulation-based dimension in cognitive radio systems to perform cooperative spectrum sharing (CSS). Unlike conventional opportunistic spectrum sharing techniques where a secondary user (SU) system attempts to utilize the spectrum hole in either time, frequency or spatial dimension created by the primary user (PU) system, this study focuses on finding accessible spectrum spaces created by the structure of modulation constellations. In this novel CSS scheme, by taking advantage of the knowledge on the PU's modulation scheme, the SU superposes its own modulated signal on the PU's signal. We examine two CSS scenarios: 1) phase-shift-keying (PSK) is used at both the PU and SU and 2) PSK is used at the PS while pulse-amplitude modulation (PAM) is used at the SU. Interestingly, the proposed superposition approach in CSS Scenario 2 enables a cooperative spectrum sharing mechanism without either impairing the performance of the primary receiver nor requiring a change in its demodulation rule. At the same time, a much better symbol-error-rate (SER) performance is achievable for the SU's receiver in Scenario 2 than in Scenario 1. Theoretical SER performances of both the PU and SU are then thoroughly analyzed and confirmed by numerical simulations.**

***Index Terms*—Cooperative spectrum sharing, symbol error rate, cognitive radio, overlay spectrum access, PSK, PAM.**

## I. Introduction

Cognitive Radio technology is a promising solution to improve the under-utilized radio spectrum resources. Dynamic spectrum access (DSA) management enables a secondary user (SU) system, also known as the cognitive system, to use the licensed spectrum of primary user (PU) systems.[1] Overlay DSA and underlay DSA are the two models which belong to the hierarchical access model in DSA. Both models have attracted a lot of research attention recently [1].

In underlay DSA, the secondary spectrum access (or unlicensed spectrum access) is allowed to happen concurrently with the primary spectrum access (or licensed spectrum access) if its interference with the PU system is below a certain interference temperature or noise-floor constraint [1]. Various methods, which applied cooperative communications into the SU system, have been proposed to reduce the such inter-system interference [2]–[11]. Note that the PU-SU collaboration is not required in underlay DSA.

In overlay DSA, there is extended cooperation between the SUs and the PU system. The secondary spectrum access is granted if certain parameters of the PU performances, *e.g.*, target achievable rates, symbol error rates (SER), interference constraint, are satisfied instead of just imposing the interference temperature constraint. Effectively, the SUs are permitted to cooperate with the PU system to actively extend its spectrum usage using frequency-based, time-based, spatial-based spectrum spaces [12]–[31]. With potentially better performances, cooperative spectrum sharing (CSS) is probably the most preferable overlay DSA scheme.

CSS methods can be categorized into two subsets. The first one is known as "green CSS" [20]–[23]. The term "green" refers to the fact that the inter-cooperation between the PU and SU systems do not cause any inter-system interferences. The spectrum sharing mechanism is based on PU and SU collaborations, which aim to create the whitespace spectrum (or clean spectrum) for the SU spectrum access. This can be done by minimizing the radio resources in time, frequency or space (T/F/S) used by the PU while still maintaining its certain target performance. Simeone *et al.* [20] proposed a sharing method that the property-right based spectrum owner (the PU system) rewards or leases the SU system an amount of saving time-resource if the cooperation satisfies the PU's target rate. Saving time resource for spectrum sharing has been attracted subsequent research on other aspects of communications such as optimizing the power consumption [22], enlarging the transmitting coverage [23] and balancing the time-base spectrum resource usage [21].

Frequency-based CSS focuses on exploiting the whitespace spectrum opportunity in the frequency dimension [25], [27]. Using orthogonal frequency-division multiplexing (OFDM), [25], [27] showed that the cooperation can save certain subcarriers used by the PU system. The surplussed subcarriers are then utilized by the SU spectrum access in the cooperating timeslot [25], [27].

Spatial dimension also offers opportunities for the green CSS if SUs are equipped with multiple antennas or multiple SUs jointly create a virtual antenna array [26], [30]. Multiple

Truc Thanh Tran is with (i) Institute of Research and Development, Duy Tan University, Vietnam, address: K7/25 Quang Trung, Danang, Vietnam; (ii) Danang Department of Information and Communication, Danang city, Vietnam (tranthanhtruc1982@gmail.com).

Duy H. N. Nguyen is with the Department of Electrical and Computer Engineering, San Diego State University, 5500 Companile Street, San Diego, CA, USA 92182 (duy.nguyen@sdsu.edu).

Ngo Van Sy is with The Central Region Center of Vietnam Research Institute of Electronics, Informations and Automation, K25/16 Ly Thuong Kiet street, Danang city, Vietnam. (singo2016@gmail.com)

Tuan Do-Hong is with Ho Chi Minh City University of Technology, Vietnam National University Ho Chi Minh City, 268 Ly Thuong Kiet street, Ho Chi Minh city, Vietnam (do-hong@hcmut.edu.vn).

[1]We use SU to refer to either the secondary transmitter or the secondary receiver in general. Similar reference is applied to the PU abbreviation.

input multiple output (MIMO) techniques are then applied to create the green spectrum or simply to mitigate the mutual interference between the PU and SU systems.

Although the green CSS provides several advantages in spectrum sharing, it imposes a burden of transmission scheduling tasks and higher adaptation ability in the PU systems. For instance, the scheduled transmission time and subcarriers must be accurately determined so that either PU or SU DSA can correctly use the spectrum without collision. Consequently, the PU-SU cooperation requires self-reconfiguring capability at the PU systems, *e.g.*, adaptive transmission timeslots and subscarriers [20], [25], [27] In addition, the findings for the green spectrum spaces in the T/F/S dimensions are always in connection with optimizing the spectrum resource, *e.g.*, minimizing the PU transmission time [20], [25], [27]. These techniques may then dramatically increase the cost and complexity of the PU systems.

The second subset of overlay DSA methods is known as "gray-spectrum-based CSS." This framework concentrates on exploiting the spectrum sharing in the same T/F/S coordinate when no possible spectrum hole is created for SU spectrum access [15]–[19]. The approach is particularly meaningful when no T/F/S spectrum hole is found or the PU systems simply do not have sufficient adaption ability and complexity to enable the green communication. Instead, the work in [15]–[19] proposed the method of exploiting the so-called "gray" spectrum spaces where the PU systems allow a certain level of acceptable interferences from the SU. The use of gray spectrum spaces, however, imposes significant limitations due to the mutual interference between the PU and SU systems, as analyzed in our recent works [12]–[14].

Motivated by the limitations of green CSS and gray-spectrum-based CSS in the T/F/S dimensions, this paper focuses on exploiting the modulation-based dimension for CSS. In this CSS method, the secondary transmitter (node R) acts as a relay to forward the signal from the primary transmitter (node S) to the primary receiver (node D), as illustrated in Fig. 1. One question arises here: what is the reward for the SU system in helping the PU system? The answer is that R can send its own signal the secondary receiver (the extra node X) on the same spectrum being used for forwarding the PU signal. Our proposed approach is based on the modulation-based dimension. Specifically, by taking advantage of the knowledge on the PU's modulation scheme, R superposes its own modulated signal on the PU's signal. In this work, we investigate the modulation-based CSS in two scenarios: 1) M-ary phase-shift-keying (PSK) is used at both the PU and SU and 2) M-ary PSK is used at the PU while M-ary pulse-amplitude modulation (PAM) is used at the SU. The main idea of this work is to exploit the property of the PSK signal when performing the spectrum sharing. Specifically, the PSK signal only locates on the angular dimension in the polar plane (the complex plane is converted to the polar plane). Therefore, a special alphabet for the SU signal can be designed to align with the radius dimension in the polar plane. In this case, the PAM signaling used by the SU in Scenario 2 can be aligned to the same phase of the PU signal. Thus, no interference from the SU signal is induced to the PU system.

The proposed approach in CSS Scenario 2 yields several important advantages, also considered as the main contributions of this study, as follows. Firstly, by smartly superimposing the SU signal over the PU signal, we show that it is possible to have DSA at a given T/F/S coordinate without interfering the PU system. Thus, the SER performance of the PU system is not degraded by the SU signal. Secondly, the proposed scheme does not require the PR to change its demodulation rule nor to do self-adaptation to the spectrum sharing context.[2] Thirdly, the proposed scheme can strengthen the received power of the PU's signal by positively aligning the SU's signal. Thus, it is capable of offering a much better performance to the PU system than a conventional CSS scheme in Scenario 1. Finally, the SER performances of both PU and SU systems are theoretically analyzed with exact expressions. Numerical simulations then confirm the SER performance advantage of the proposed modulation-based CSS.

The remainder of the article is organized as follows. Section II introduces the system model which includes the description about the system configuration, assumptions in use and notations. Section III refers to the conventional cooperative spectrum scheme (Scenario 1) which is presented to compare with the proposed method in Scenario 2. Section IV describes the details of the proposed method, which is referred to as the modulation-based CSS. The comparison between two approaches are then performed in Section IV. Section V provides the simulation results and discussion. Concluding remarks of our study are given in Section VI.

## II. System Model

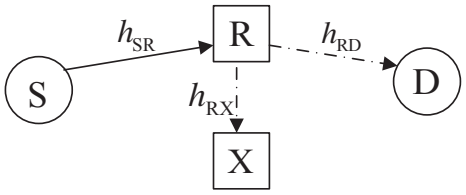


Fig. 1. Diagram of a CSS system where node R concurrently assists the S $\rightarrow$ D communication and sends its own signal to node X.

We consider an overlay DSA cognitive radio system with four nodes S, D, R and X, each equipped with one antenna as illustrated in Fig. 1. The source node S and destination node D are the PUs of the spectrum. The S $\rightarrow$ D communication is assisted by the half-duplex relay node R. Specifically, the

[2]Previous work in the green CSS model requires the PU system to strictly follow the saving T/F/S resources that are created by the collaborated SU system.

relay R listens to the source S in the first time slot and forwards the decoded message to the destination D in the second time slot. In this second time slot, R also tries to send its signal to its intended receiver, the extra node X. Herein, R and X act as SUs. We denote $h_{ij}$ as the channel coefficient between any node $i$ and $j$, where $i, j \in \{\mathrm{S}, \mathrm{D}, \mathrm{R}, \mathrm{X}\}$.

Define $\mathcal{S}_{\mathrm{PSK}} = \left\{\tilde{S}_m \middle| \tilde{S}_m = \mathrm{e}^{-\mathrm{i}\varphi_m}, 0 \le m \le M-1\right\}$ with $\varphi_m = \frac{2\pi m}{M}$ as an $M$-symbol PSK alphabet used by the PU. On the other hand, the SU can use either:

- An $N$-symbol PSK alphabet $\mathcal{U}_{\mathrm{PSK}} = \left\{U_n \middle| U_n = \mathrm{e}^{-\mathrm{i}\frac{2\pi n}{N}}, 0 \le n \le N-1\right\}$
- Or an $N$-symbol PAM alphabet $\mathcal{U}_{\mathrm{PAM}} = \left\{U_n \middle| U_n = \frac{2n-N+1}{\sqrt{(N^2-1)/3}}, 0 \le n \le N-1\right\}$.

Our investigation on the joint spectrum utilization between the PU and SU is based on the following assumptions:

*i.* The baseband noise at an any node is complex Gaussian with zero mean and unit variance.

*ii.* The channel coefficients $h_{ij}$ (except $h_{\mathrm{SD}}$) are perfectly estimated and globally known by all nodes. For each period of transmission time (including two timeslots), $h_{ij}$ is assumed to be invariant. The direct transmission path between S and D is unavailable, leading to the need for collaboration from the SU system to relay the PU signal

*iii.* The transmission time consists of two timeslots (TSL): the broadcasting and forwarding timeslots (B-TSL and F-TSL). In the B-TSL, S broadcasts the PU signal. R employs the decode-and-forward (DF) protocol by first decoding the PU signal. If the decoding is successful, R then regenerates the PU signal and forwards it to D in the F-TSL.[3] At the same time, R tries to superimpose its own signals (intended for its receiver X) over the forwarded signal intended for D. In doing so, R opportunistically accesses the licensed spectrum owned by the PU system S–D. The PU system allows the spectrum sharing under a condition that the signal to interference and noise ratio (SINR) at D, namely $\gamma_{\mathrm{D}}$, is above a certain value $\gamma_0$:

$$\gamma_{\mathrm{D}} \ge \gamma_0. \tag{1}$$

In this study, we focus on the spectrum sharing when $\gamma_0 \gg 1$, which is a common requirement in practice to guarantee acceptable performance at the PU receiver.

*iv.* The spectrum sharing only occurs when the source message is correctly decoded at R. Otherwise, R simply stays idle in the F-TSL phase. It might be argued why the SU system does not use spectrum for its own signal transmission in this case. In fact, several previous studies have appealed for the SU's right of using the spectrum even when the collaboration fails [18], [19]. However, with the superposition of the PU and SU signals considered in this work, if there is no PU signal, the PU receiver D will mistakenly decode the SU signal. As a result, the PU system performance will significantly degrade. For this reason, we make the assumption that SU transmitter R stays silent in this case.

[3]It is assumed that the relay node R is capable of performing error detection and correction to the source signal.

## III. Cooperative Spectrum Sharing Scenario 1: PSK Signaling at the SU System

This section investigates the spectrum sharing between the PU and SU systems where PSK signaling is utilized at both systems. However, we assume that the two systems use two different sets of basis functions. We denote $\Phi$ and $\Psi$ as the basis function sets of the PU and SU systems, respectively. At the transmitter of each system (*i.e.*, S or R), the transmitted waveforms are constructed by mapping its binary information sequence into its corresponding basis function set [32]. At the receiver of each system (*i.e.*, D or X), a correlation (or matched-filter) demodulator is imposed on the received signal to extract the baseband symbol [32].

The reasons for our assumptions of using different sets of basis functions at the PU and SU systems are two-fold. First, the cross-correlation between the waveforms representing the PU and SU symbols might be reduced even though node R superimposes the SU symbol over the PU symbol in the B-TSL timeslot. Second, the amount of interfering signal incurred after the baseband demodulation stage, *e.g.*, the undesirable SU signal with respect to (w.r.t) the extraction of PU signal at node D, can be modeled as a complex Gaussian random variable (RV). This is because the interfering signal shape is unpredictably distorted due to different basis function sets [33], [34]. We note that the assumption of Gaussian interference sources also enable our analysis on the performances of the PU and SU systems in Section V.

Denote $\tilde{S}_m$ as the PU symbol which was correctly decoded by node R and $U_n$ as the SU symbol intended for node X. Denote $P_1$ as the power budget at node R. Node R then allocates $P_1^{\mathrm{P}}$ and $P_1^{\mathrm{S}}$ as the transmit powers for the PU and SU symbols, respectively. R then maps $\tilde{S}_m$ into a bandpass signal $\sqrt{P_1^{\mathrm{P}}}\tilde{s}_m(t)$ using the basis function set $\Phi$. Similarly, $U_n$ is mapped into a bandpass signal $\sqrt{P_2^{\mathrm{S}}}u_n(t)$ using the basis function set $\Psi$. The two bandpass signals are then superimposed with each other and broadcast by the node R to both D and X as a composite signal $\sqrt{P_1^{\mathrm{P}}}\tilde{s}_m(t)+\sqrt{P_1^{\mathrm{S}}}u_n(t)$.

### A. Baseband Symbol Demodulation at D

At node D, the received bandpass signal can be model as $y_{\mathrm{D}}(t) = h_{\mathrm{RD}}\sqrt{P_1^{\mathrm{P}}}\tilde{s}_m(t) + h_{\mathrm{RD}}\sqrt{P_1^{\mathrm{S}}}u_n(t) + z_{\mathrm{D}}(t)$, where $z_{\mathrm{D}}(t)$ is the AWGN process at node D. Projecting the received signal onto the basis function set $\Phi$ of the PU system, the baseband signal is given by

$$\begin{aligned} y_{\mathrm{D}} &= h_{\mathrm{RD}}\sqrt{P_1^{\mathrm{P}}}\tilde{S}_m + h_{\mathrm{RD}}\sqrt{P_1^{\mathrm{S}}}\bar{u}_n + z_{\mathrm{D}} \\ \Leftrightarrow \tilde{y}_{\mathrm{D}} &= \frac{y_{\mathrm{D}}}{h_{\mathrm{RD}}} = \sqrt{P_1^{\mathrm{P}}}\tilde{S}_m + \sqrt{P_1^{\mathrm{S}}}\bar{u}_n + \tilde{z}_{\mathrm{D}}, \end{aligned} \tag{2}$$

where $\bar{u}_n$ denotes the baseband interference created by projecting the bandpass SU signal $u_n(t)$ onto the basis function set $\Phi$ and $z_{\mathrm{D}} \sim \mathcal{CN}(0,1)$ is the baseband AWGN. As

aforementioned, we model $\bar{u}_n$ as a complex Gaussian RV $\bar{u}_n \sim \mathcal{CN}(0,1)$, similarly to [33], [34]. $\tilde{z}_{\rm D}$ is defined as $\frac{z_{\rm D}}{h_{\rm RD}}$, which makes $\tilde{z}_{\rm D} \sim \mathcal{CN}\left(0,\sigma_{\rm D}^2\right)$, where $\sigma_{\rm D} = \frac{1}{|h_{\rm RD}|}$.

Since node D is the PU, its operation should not be affected by the appearance of the SU system. Thus, node D only attempts to demodulate the PU symbol using the denoted rule $R_1$ as given in (3).

**Algorithm 1:** The PU symbol demodulation at D in CSS Scenario 1 (Rule $R_1$)

Perform the Maximum Likelihood (ML) Demodulation

$$\breve{m} = \underset{0\le \dot{m}\le M-1}{\arg\min} \left\{ \left\| \tilde{y}_{\rm D} - \sqrt{P_1^{\rm P}}\tilde{S}_{\dot{m}} \right\| \right\}. \tag{3}$$

The SER in demodulating a PSK signal at D, denoted as $P_{e,\rm D}^*(\gamma_{\rm D})$, is then given by [32]

$$P_{e,\rm D}^*(\gamma_{\rm D}) \triangleq \Pr\{\breve{m} \neq m \,|F_m\} = 2Q\Big(\sqrt{2\gamma_{\rm D}}\sin\frac{\pi}{M}\Big), \tag{4}$$

where $F_m$ denotes the event that S transmits the $m$th symbol $\tilde{S}_m$, and $\gamma_{\rm D} = \frac{|h_{\rm RD}|^2 P_1^{\rm P}}{|h_{\rm RD}|^2 P_1^{\rm S}+1}$ is the SINR at D. It is easy to see that $P_1^{\rm S}$ should be smaller than $P_1^{\rm P}$ to have a good SER performance at D.

### *B. Baseband Symbol Demodulation at* X

Since node X is a cognitive SU and the SU signal is likely much smaller than the PU signal, we assume certain successive interference cancellation capability at node X. In this case, node X has to possess the basis function sets of both the PU and SU systems.

Denote $y_{\rm X}(t) = h_{\rm RX}\sqrt{P_1^{\rm P}}\tilde{s}_m(t) + h_{\rm RX}\sqrt{P_1^{\rm S}}u_n(t) + z_{\rm X}(t)$ as the received bandpass signal at X and $z_{\rm X}(t)$ as the AWGN process. X performs the projections of the received bandpass signal, onto each basis function sets, $\Phi$ and $\Psi$, to create the baseband signals. Specifically, the projection of $y_{\rm X}(t)$ onto $\Phi$ yields

$$\begin{aligned} \dot{y}_{\rm X} &= h_{\rm RX}\sqrt{P_1^{\rm P}}\tilde{S}_m + h_{\rm RX}\sqrt{P_1^{\rm S}}\bar{u}_n + \dot{z}_{\rm X} \\ \Leftrightarrow \tilde{y}_{\rm X} &= \frac{\dot{y}_{\rm X}}{h_{\rm RX}} = \sqrt{P_1^{\rm P}}\tilde{S}_m + \sqrt{P_1^{\rm S}}\bar{u}_n + \tilde{z}_{\rm X}, \end{aligned} \tag{5}$$

which is used for PU symbol demodulation. Herein, $\bar{u}_n$ and $\dot{z}_{\rm X} \sim \mathcal{CN}(0,1)$ are the SU symbol and the baseband AWGN w.r.t the projection onto $\Phi$. Thus, $\tilde{z}_{\rm X} = \frac{\dot{z}_{\rm X}}{h_{\rm RX}}$ is complex Gaussian distributed $\tilde{z}_{\rm X} \sim \mathcal{CN}\left(0,\sigma_{\rm X}^2\right)$ with $\sigma_{\rm X} = \frac{1}{|h_{\rm RX}|}$. Similarly, the projection of $y_{\rm X}$ onto $\Psi$ creates the received baseband signal

$$\begin{aligned} \ddot{y}_{\rm X} &= h_{\rm RX}\sqrt{P_1^{\rm S}}U_n + h_{\rm RX}\sqrt{P_1^{\rm P}}\bar{s}_m + \ddot{z}_{\rm X} \\ \Leftrightarrow \hat{y}_{\rm X} &= \frac{\ddot{y}_{\rm X}}{h_{\rm RX}} = \sqrt{P_1^{\rm S}}U_n + \sqrt{P_1^{\rm P}}\bar{s}_m + \frac{\ddot{z}_{\rm X}}{h_{\rm RX}}, \end{aligned} \tag{6}$$

which is used for SU symbol demodulation. Herein, $\bar{s}_m$ denotes the baseband signal resulting from projecting the bandpass signal $\tilde{s}_m(t)$ onto $\Psi$ and is modeled as a complex Gaussian RV $\mathcal{CN}(0,1)$ and $\ddot{z}_{\rm D} \sim \mathcal{CN}(0,1)$ is the baseband AWGN w.r.t the projection of the bandpass noise onto $\Psi$.

In doing SIC, X prioritizes the demodulation of the stronger signal. Since it is very likely that $P_1^{\rm P} > P_1^{\rm S}$, X will demodulate the PU signal first. The procedure of demodulating the PU signal and subsequently the SU signal, denoted as Rule $R_2$, is summarized in Algorithm 2. For completeness, we also consider the case $P_1^{\rm S} \ge P_1^{\rm P}$ where X only attempts to demodulate the SU symbol.

**Algorithm 2:** The SU symbol demodulation at X in CSS Scenario 1 (Rule $R_2$)

**for** $P_1^{\rm P} > P_1^{\rm S}$ **do**

Estimate the PU symbol:

$$\bar{\breve{m}} = \underset{0\le \dot{m}\le M-1}{\arg\min} \left\{ \left\| \tilde{y}_{\rm X} - \sqrt{P_1^{\rm P}}\tilde{S}_{\dot{m}} \right\| \right\}. \tag{7}$$

Reconstruct the baseband interference signal $\bar{s}_{\bar{\breve{m}}}$ from $\tilde{S}_{\bar{\breve{m}}}$;

Cancel the interference (the PU baseband signal) in $\tilde{y}_{\rm X}$ based on $\bar{s}_{\bar{\breve{m}}}$:

$$\widehat{y}_{\rm X} = \hat{y}_{\rm X} - \sqrt{P_1^{\rm P}}\bar{s}_{\bar{\breve{m}}}. \tag{8}$$

ML demodulation of the SU symbol

$$\bar{\bar{n}} = \underset{0\le \dot{n}\le N-1}{\arg\min} \left\{ \left\| \widehat{y}_{\rm X} - \sqrt{P_1^{\rm S}}U_{\dot{n}} \right\| \right\}. \tag{9}$$

**end**

**for** $P_1^{\rm S} \ge P_1^{\rm P}$ **do**

ML demodulation of the SU symbol

$$\bar{\bar{n}} = \underset{0\le \dot{n}\le N-1}{\arg\min} \left\{ \left\| \hat{y}_{\rm X} - \sqrt{P_1^{\rm S}}U_{\dot{n}} \right\| \right\}. \tag{10}$$

**end**

Note that if a high target SINR is set at the PU receiver D, *i.e.*, $\gamma_0 \gg 1$, X has to use the demodulation rule with $P_1^{\rm P} \gg P_1^{\rm S}$. Thus, the SER in demodulating the SU's PSK symbol using SIC can be expressed as

$$\begin{aligned} P_{e,\rm X}^* &\overset{P_1^{\rm P}>P_1^{\rm S}}{=} \frac{1}{N}\sum_{n=0}^{N-1} \Pr\{\bar{\bar{n}} \neq n \big| R_2, F_m, \dot{G}_n, P_1^{\rm P} > P_1^{\rm S}\} \\ &= \frac{1}{N}\sum_{n=0}^{N-1} \Big( \Pr\{\bar{\bar{n}} \neq n, \bar{\breve{m}} = m \big| R_2, F_m, \dot{G}_n, P_1^{\rm P} > P_1^{\rm S}\} \\ &\quad + \Pr\{\bar{\bar{n}} \neq n, \bar{\breve{m}} \neq m \big| R_2, F_m, \dot{G}_n, P_1^{\rm P} > P_1^{\rm S}\} \Big), \end{aligned} \tag{11}$$

where $\dot{G}_n$ is denoted as the event that R transmits $U_n$.

## IV. Cooperative Spectrum Sharing Scenario 2: PAM Signaling at the SU System

In this section, we examine the spectrum sharing scenario where PAM signaling is employed at the SU system. With PAM signaling, the $M$-ary alphabet $\mathcal{S}_{\rm PAM} = \{U_n, 0 \le n \le N-1\}$ with $N$ symbols is constructed as

$$U_n = \frac{2n-N+1}{\sqrt{(N^2-1)/3}}, 0 \le n \le N-1. \tag{12}$$

We assume equiprobablity for each symbol in the alphabet, $\mathbb{E}\{U_n\} = 0$ and $\mathbb{E}\{|U_n|^2\} = 1$. Node R then superimposes

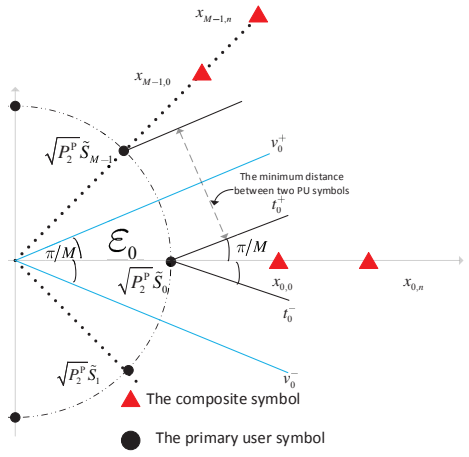


Fig. 2. The cooperative modulation approach to create the composite PU&SU signal

the SU's PAM symbol onto the PU's PSK symbol. In general, PAM is less energy-efficient than PSK [32]. In this work, our aim is to show that the CSS Scenario 2 with PAM signaling is capable of outperforming the CSS Scenario 1 with PSK signaling.

Fig. 2 illustrates an example of generating the transmitted symbol at R based on the proposed cooperative modulation scheme, where $x_{m,n}$, $0 \le m \le M-1$, $0 \le n \le N-1$, is a composite symbol. Having correctly decoded the PU's PSK symbol $\tilde{S}_m$, the SU's PAM symbol is first rotated to the phase of $\tilde{S}_m$ and then superimposed onto $\tilde{S}_m$. Mathematically, the composite PSK and PAM signal to be transmitted by R can be expressed as

$$\begin{aligned} x_{m,n} &= \left(\sqrt{P_2^{\mathrm{P}}} + \sqrt{t} + \sqrt{P_2^{\mathrm{S}}}U_n\right) \exp\left(-\mathbb{i}\frac{2\pi m}{M}\right) \\ &= \left(\sqrt{P_2^{\mathrm{P}}} + \sqrt{t} + \sqrt{P_2^{\mathrm{S}}}U_n\right)\tilde{S}_m, \end{aligned} \tag{13}$$

where $P_2^{\mathrm{P}}$ and $P_2^{\mathrm{S}}$ are the allocated powers for the PU's and SU's signals, respectively, and $t$ is an additional factor that allows the SU symbol to constructively strengthen the PU symbol. Note that the settings of $P_2^{\mathrm{P}}$, $P_2^{\mathrm{S}}$ and $t$ affect the power consumption at X as well as the performance of both PU and SU systems.

By properly setting $t$, the constructive alignment of the SU's PAM signaling yields several benefits the SU's PSK signaling. First, the phase of the composite signal is the same as the phase of the PU's PSK symbol. The demodulation rule as the PU's receiver D, which is based on phase detection, is therefore unchanged. Second, the presumptive "interference" from the SU's signal does push the composite signal further away from the origin. Effectively, this procedure increases the SNR of PU's PSK signaling. As being shown in the Fig. 2, if a composite symbol $x_{0,n}$ is transmitted, the distances to the decision boundaries $Ov_0^+$ and $Ov_0^-$ will be enlarged due to the superposition of the PAM signaling, compared to the distances from the original PSK signal $\tilde{S}_0$. Thus, the SER of the PU's signaling is potentially reduced by the proposed scheme. Note that in order to the constructive interference from the SU's signaling, the SU system has to use the same basis function set $\Phi$ as the PU system. This aspect is different to the CSS Scenario 1.

### A. Baseband Symbol Detection at D

At node R, the composite symbol $x_{m,n}$ is converted into a bandpass signal for transmission using the basis function $\Phi$ and transmitted to the both nodes D and X. At node D, the received baseband signal $y_{\mathrm{D}}$ is given by

$$\begin{aligned} y_{\mathrm{D}}\left(\tilde{S}_m, U_n\right) &= h_{\mathrm{RD}} x_{m,n} + z_{\mathrm{D}} \\ \Leftrightarrow \tilde{y}_{\mathrm{D}}\left(\tilde{S}_m, U_n\right) &= \frac{y_{\mathrm{D}}\left(\tilde{S}_m, U_n\right)}{h_{\mathrm{RD}}} \\ &= \left(\sqrt{P_2^{\mathrm{P}}} + \sqrt{t} + \sqrt{P_2^{\mathrm{S}}}U_n\right)\tilde{S}_m + \tilde{z}_{\mathrm{D}}, \end{aligned} \tag{14}$$

where $\tilde{z}_{\mathrm{D}}$ is the effective AWGN. The symbol demodulation rule at D is the same as that in Scenario 1, *i.e.*, Rule $R_1$ in Algorithm 1. Thus, the demodulation rule at R is

$$\breve{m} = \underset{0 \le \dot{m} \le M-1}{\arg\min} \left\{ \left\| \tilde{y}_{\mathrm{D}}\left(\tilde{S}_m, U_n\right) - \sqrt{P_2^{\mathrm{P}}}\tilde{S}_{\dot{m}} \right\| \right\}. \tag{15}$$

In order to achieve the target SNR of $\gamma_0$ at the D, the minimum allocated power $P_2^{\mathrm{P}}$ for the SU signal is $\gamma_0/|h_{\mathrm{RD}}|^2$. Thus, node D can set $P_2^{\mathrm{P}} = \gamma_0/|h_{\mathrm{RD}}|^2$ in its detection decision (15). Although $\left|\sqrt{P_2^{\mathrm{P}}} + \sqrt{t} + \sqrt{P_2^{\mathrm{S}}}U_n\right|^2$ is the true transmit power at R, the PU may not have the knowledge of this transmit power. However, the demodulation of the PSK signaling based on the receive signal phase, should not be affected by the absence of the received signal amplitude. The SER at D in this scenario, denoted as $P_{e,\mathrm{D}}^{**}$, can be expressed as

$$P_{e,\mathrm{D}}^{**} \triangleq \Pr\{\breve{m} \ne m \,|F_m\}. \tag{16}$$

### B. Baseband symbol detection at X

At node X, the received signal is projected onto the basis function set $\Phi$ to recover the baseband signal. The received baseband signal is then given by:

$$\begin{aligned} y_{\mathrm{X}}\left(\tilde{S}_m, U_n\right) &= h_{\mathrm{RX}} x_{m,n} + z_{\mathrm{X}} \\ \Leftrightarrow \tilde{y}_{\mathrm{X}}\left(\tilde{S}_m, U_n\right) &= \frac{y_{\mathrm{X}}\left(\tilde{S}_m, U_n\right)}{h_{\mathrm{RX}}} \\ &= \left(\sqrt{P_2^{\mathrm{P}}} + \sqrt{t} + \sqrt{P_2^{\mathrm{S}}}U_n\right)\tilde{S}_m + \tilde{z}_{\mathrm{X}}, \end{aligned} \tag{17}$$

where $\tilde{z}_{\mathrm{X}} \sim \mathcal{CN}\left(0, \frac{1}{|h_{\mathrm{RX}}|^2}\right)$ is the AWGN at X. Since the SU's PAM symbol is embedded in the phase of the PU's PSK symbol, X has to use SIC. Specifically, X detects the phase of the PU's PSK symbol and then removes the estimated symbol from the received signal. The SU's receiver X then proceed to demodulate its intended $\mathcal{S}_{\mathrm{PAM}}$. This SIC demodulation procedure is summarized in Algorithm 3.

**Algorithm 3:** The SU symbol demodulation at X in CSS Scenario 2 (Rule $R_3$)

1 Demodulate the PU's PSK symbol

$$\bar{\bar{m}} = \underset{0\le \dot{m}\le M-1}{\arg\min} \left\{ \left\| \tilde{y}_{\rm X}\left(\tilde{S}_m, U_n\right) - \sqrt{P_2^{\rm P}}\tilde{S}_{\dot{m}} \right\| \right\}. \quad (18)$$

2 Remove the PU's signal in $\tilde{y}_{\rm X}$ using the estimated PU symbol

$$\widehat{y}_{\rm X}\left(\tilde{S}_m, U_n, \tilde{S}_{\bar{\bar{m}}}\right) = \Re\left\{ \frac{\tilde{y}_{\rm X}\left(\tilde{S}_m, U_n\right)}{\tilde{S}_{\bar{\bar{m}}}} \right\} - \sqrt{P_2^{\rm P}} - \sqrt{t}. \quad (19)$$

3 Demodulate the SU's PAM symbol based on $\widehat{y}_{\rm X}$

$$\bar{\bar{n}} = \underset{0\le \dot{n}\le N-1}{\arg\min} \left\{ \left\| \widehat{y}_{\rm X}\left(\tilde{S}_m, U_n, \tilde{S}_{\bar{\bar{m}}}\right) - \sqrt{P_2^{\rm S}}U_{\dot{n}} \right\| \right\}. \quad (20)$$

Using rule $R_3$, the SER in demodulating the SU symbol, denoted as $P_{e,{\rm X}}^{**}$, is given by

$$P_{e,{\rm X}}^{**} = \frac{1}{N}\sum_{n=0}^{N-1} \Pr\left\{ \bar{\bar{n}} \neq n \,\middle|\, R_3, F_m, \dot{G}_n \right\}, \quad (21)$$

where $\dot{G}_n$ is the event of transmitting PAM symbol $U_n$.

## V. Comparison of SER Performances in CSS Scenarios 1 and 2

This section presents the SER performance analysis of the PU and SU systems in both CSS Scenarios 1 and 2. Since the PU symbols are equiprobable, we assume that $\tilde{S}_0 \in \mathcal{S}_{\rm PSK}$ is the transmitted PSK symbol without loss of generality. Thus, the composite symbol transmitted by R in the F-TSL is $x_{0,n} = \left(\sqrt{P_2^{\rm P}} + \sqrt{t} + U_n\sqrt{P_2^{\rm S}}\right)$ in CSS Scenario 2.

### A. SER Performances at D

In this part, we analyze and compare the SERs at node D in CSS Scenarios 1 and 2. We then establish the condition on the allocated power for the PU symbol at node R such that the SER performance in CSS Scenario 2 is superior to that in CSS Scenario 1.

*1) SER Performance at* D *in CSS Scenario 1:* Referring to Equation (4), the SER at D in CSS Scenario 1 is given by $P_{e,{\rm D}}^{*}(\gamma_0) = 2Q\left(\sqrt{2\gamma_0}\sin\frac{\pi}{M}\right)$ for $\gamma_{\rm D} = \gamma_0$. Because $P_{e,{\rm D}}^{*}(\gamma_{\rm D})$ in a decreasing function in $\gamma_{\rm D}$, one has $P_{e,{\rm D}}^{*}(\gamma_{\rm D}) \le P_{e,{\rm D}}^{*}(\gamma_0)$ under the condition $\gamma_{\rm D} \ge \gamma_0$. Therefore, we use $P_{e,{\rm D}}^{*}(\gamma_0)$ as the baseline for evaluating the SER performance at D. If the CSS Scenario 2 is better than the CSS Scenario 1, one definite requirement for the SER performance at D is $P_{e,{\rm D}}^{**} \le P_{e,{\rm D}}^{*}(\gamma_0)$.

*2) SER Performance at* D *in CSS Scenario 2:* Let $\mathcal{E}_0$ be the region in-bounded by the two rays $Ov_0^-$ and $Ov_0^+$, as being shown in Fig. 2. As long as the received signal at D inside $\mathcal{E}_0$, it is possible to correctly demodulate the PU symbol as $\tilde{S}_0$. Thus, the SER in demodulating the PU's PSK symbol at D can be rewritten as

$$P_{e,{\rm D}}^{**} = \frac{1}{N}\sum_{n=0}^{N-1} \Pr\left\{ \tilde{y}_{\rm D}\left(\tilde{S}_0, U_n\right) \notin \mathcal{E}_0 \right\} \quad (22)$$
$$= \frac{1}{N}\sum_{n=0}^{N-1} \underbrace{2Q\left(\sqrt{2\gamma_{{\rm D},n}}\sin\frac{\pi}{M}\right)}_{H_{\rm D}(\gamma_{{\rm D},n})} = \frac{1}{N}\sum_{n=0}^{N-1} H_{\rm D}\left(\gamma_{{\rm D},n}\right),$$

where

$$\gamma_{{\rm D},n} = \frac{x_{0,n}^2}{\sigma_{\rm X}^2} = \frac{\left(\sqrt{P_2^{\rm P}} + \sqrt{t} + \sqrt{P_2^{\rm S}}U_n\right)^2}{\sigma_{\rm D}^2}$$
$$= \left|h_{\rm RD}\right|^2\left(\sqrt{P_2^{\rm P}} + \sqrt{t} + \sqrt{P_2^{\rm S}}U_n\right)^2. \quad (23)$$

By the construction of PAM symbols $U_n$'s in (12), one has

$$\gamma_{{\rm D},0} < \ldots < \gamma_{{\rm D},\frac{N}{2}} < \left|h_{\rm RD}\right|^2\left(\sqrt{P_2^{\rm P}} + \sqrt{t}\right)^2$$
$$< \gamma_{{\rm D},\frac{N}{2}+1} < \ldots < \gamma_{{\rm D},N-1}. \quad (24)$$

**Proposition 1.** *For $t \ge 3P_2^{\rm S}\frac{N-1}{N+1}$, the SER in demodulating the PU symbol in CSS Scenario 2 does not exceed that in CSS Scenario 1 with target SINR $\gamma_0$, i.e.,*

$$P_{e,{\rm D}}^{**} \le P_{e,{\rm D}}^{*}\left(\gamma_0\right). \quad (25)$$

*Proof:* From (23), the event, $\gamma_{{\rm D},0} \ge \gamma_0$, occurs when $\left|h_{\rm RD}\right|^2\left|\sqrt{P_2^{\rm P}} + \sqrt{t} + \sqrt{P_2^{\rm S}}U_n\right|^2 \ge \gamma_0$. Because $\gamma_0 = \left|h_{\rm RD}\right|^2 P_2^{\rm P}$, this is then equivalent to the condition $t \ge 3P_2^{\rm S}\frac{N-1}{N+1}$.

From (4), $\gamma_{{\rm D},0} \ge \gamma_0 \Rightarrow H_{\rm D}\left(\gamma_{{\rm D},n}\right) \le P_{e,{\rm D}}^{*}\left(\gamma_0\right), \forall 0 \le n \le N-1$. Based on (22), the proposition follows. ∎

*Remark 1:* We enforce the condition $t \ge 3P_2^{\rm S}\frac{N-1}{N+1}$ to guarantee the superior SER performance of the CSS Scenario 2, compared to the CSS Scenario 1. In particular, we let $t = 3P_2^{\rm S}\frac{N-1}{N+1} + kP_2^{\rm S}$, where $k > 0$ is an adjustable system parameter. The higher $k$ is, the better performance of the CSS Scenario 2 is, at the cost of increasing the transmit power at R. To this end, the comparisons between the two scenarios focus on two remaining aspects: the SER performances at X and the power consumptions at R.

### B. SER Performances at X

*1) SER Performance at* X *in CSS Scenario 1:* In this section, we attempt to derive lower bounds on the SER performance of SU node X under the CSS Scenario 1.

**Proposition 2.** *For $\gamma_0 \gg 1$, the SER at* X *in Scenario 1, $P_{e,{\rm X}}^{*}$, is lower-bounded as follows:*

$$P_{e,{\rm X}}^{*} \ge P_{e,{\rm X}}^{*,{\rm low}} \triangleq \max\left\{\bar{P}_{e,{\rm X}}^{*}, \hat{P}_{e,{\rm X}}^{*}\right\}, \quad (26)$$

*$\bar{P}_{e,{\rm X}}^{*}$, where $\bar{P}_{e,{\rm X}}^{*} = 2Q\left(\sqrt{2\gamma_{\rm X}}\sin\frac{\pi}{M}\right)$ and $\gamma_{\rm X} = \frac{P_1^{\rm P}}{P_1^{\rm S}+\sigma_{\rm X}^2} = \frac{\left|h_{\rm RX}\right|^2 P_1^{\rm P}}{\left|h_{\rm RX}\right|^2 P_1^{\rm S}+1}$, is the SER of detecting the PU symbol at* X *w.r.t the detection rule $R_2$ when $P_1^{\rm P} > P_1^{\rm S}$. $\hat{P}_{e,{\rm X}}^{*}$ represents the SER of detecting the SU symbol at* X *w.r.t the*

*detection rule $R_2$ when setting $P_1^{\mathrm{P}} = 0$ and $P_1^{\mathrm{S}} > 0$. $\hat{P}_{e,\mathrm{X}}^* = 2Q\big(\sqrt{2\hat{\gamma}_{\mathrm{X}}}\sin\big(\frac{\pi}{N}\big)\big)$ for a conventional $M$-ary PSK modulation, where $\hat{\gamma}_{\mathrm{X}} = |h_{\mathrm{RX}}|^2 P_1^{\mathrm{S}}$.*

*Proof:* When $\gamma_0 \gg 1$, node $D$ must allocate much higher power for PU signal than for SU signal, *i.e.*, $P_1^{\mathrm{P}} \gg P_1^{\mathrm{S}}$. Under this condition, if X fails to correctly detect the PU symbol and remove the PU's interference in $\widehat{y}_{\mathrm{X}}$, the post-SIC SINR of SU signaling at X will be very low. As a result, $\Pr\{\bar{\bar{n}} \neq n \big| \bar{\bar{m}} \neq 0, R_2, F_0, \dot{G}_n\} \approx 1$ for $\gamma_0 \gg 1$. Therefore,

$$\begin{aligned}\frac{1}{N}\sum_{n=0}^{N-1} &\Pr\{\bar{\bar{n}} \neq n \big| \bar{\bar{m}} \neq 0, R_2, F_0, \dot{G}_n, P_1^{\mathrm{P}} > P_1^{\mathrm{S}}\} \\ &\times \Pr\{\bar{\bar{m}} \neq 0 \big| R_2, F_0, \dot{G}_n, P_1^{\mathrm{P}} > P_1^{\mathrm{S}}\} \\ &\approx \Pr\{\bar{\bar{m}} \neq 0 \big| R_2, F_0\} = \bar{P}_{e,\mathrm{X}}^*. \end{aligned} \tag{27}$$

As a result, from (11), $P_{e,\mathrm{X}}^*$ can be approximated as follows:

$$\begin{aligned} P_{e,\mathrm{X}}^* \overset{\gamma_0 \gg 1}{\approx} \frac{1}{N}\sum_{n=0}^{N-1} &\Big(\Pr\big\{\bar{\bar{n}} \neq n \big| \bar{\bar{m}} = 0, R_2, F_m, \dot{G}_n, P_1^{\mathrm{P}} > P_1^{\mathrm{S}}\big\} \\ &\times \Pr\{\bar{\bar{m}} = 0 \big| R_2, F_m, \dot{G}_n, P_1^{\mathrm{P}} > P_1^{\mathrm{S}}\}\Big\} \\ &+ \Pr\{\bar{\bar{m}} \neq 0 \big| R_2, F_m\} \\ \geq\ & \Pr\{\bar{\bar{m}} \neq 0 \big| R_2, F_m\} = \bar{P}_{e,\mathrm{X}}^*. \end{aligned} \tag{28}$$

In case R does not perform any collaboration, the SU signal will be transmitted at node D's power limit, *i.e.*, $P_1^{\mathrm{S}} = P_1$ while $P_1^{\mathrm{P}}$ is set at 0. Thus, the SER in detecting the SU signal is not affected by any interference from the PU signal. As a result, $\hat{P}_{e,\mathrm{X}}^*$ achieved with $P_1^{\mathrm{P}} = 0$ must be a lower-bound for the SER $P_{e,\mathrm{X}}^*$ in case of spectrum sharing and collaboration at R ($P_1^{\mathrm{P}} > 0$). Consequently, the proposition is proved. ∎

Proposition 2 established lower bounds on the SER in demodulating the SU symbol. This bound can be minimized as being shown in the next proposition.

**Proposition 3.** *Given $P_1$ as the power budget at* R*, setting $P_1^{\mathrm{S}} = P_{1,\mathrm{opt}}^{\mathrm{S}}$, where $P_{1,\mathrm{opt}}^{\mathrm{S}}$ is given in Equation* (30) *at the top of the next page, will minimize $P_{e,\mathrm{X}}^{*,\mathrm{low}}$. The achievable minimum SER, denoted as $P_{e,\mathrm{X},\min}^{*,\mathrm{low}}$, is given by*

$$P_{e,\mathrm{X},\min}^{*,\mathrm{low}} = 2Q\left(\sqrt{2P_{1,\mathrm{opt}}^{\mathrm{S}}\left|h_{\mathrm{RX}}\right|^2}\sin\frac{\pi}{N}\right). \tag{29}$$

*Proof:* First of all, the SINR constraint (1) at node D implies $0 \leq P_1^{\mathrm{S}} \leq P_{1,b}^{\mathrm{S}}$ where

$$P_{1,b}^{\mathrm{S}} = \frac{P_1}{1+\gamma_0} - \frac{\gamma_0}{\left|h_{\mathrm{RD}}\right|^2(1+\gamma_0)}. \tag{31}$$

We now examine the two lower-bounds, $\bar{P}_{e,\mathrm{X}}^*$ and $\hat{P}_{e,\mathrm{X}}^*$, of $P_{e,\mathrm{X}}^{**}$ given in (26). Note that $\bar{P}_{e,\mathrm{X}}^*$ is an increasing function, while $\hat{P}_{e,\mathrm{X}}^*$ is a decreasing function in $P_1^{\mathrm{S}}$. The two functions intersect at $P_1^{\mathrm{S}} = P_{1,a}^{\mathrm{S}}$, where $P_{1,a}^{\mathrm{S}}$ is a root of the following equation:

$$(P_1^{\mathrm{S}})^2\left|h_{\mathrm{RX}}\right|^2\sin^2\frac{\pi}{N} + P_1^{\mathrm{S}}\left(\sin^2\frac{\pi}{M} + \sin^2\frac{\pi}{M}\right) - P_1\sin^2\frac{\pi}{N} = 0. \tag{32}$$

The sole positive root of this equation is given in (30).

We consider two cases:

1) $0 \leq P_{1,a}^{\mathrm{S}} \leq P_{1,b}^{\mathrm{S}}$: in this case, $P_{1,\mathrm{opt}}^{\mathrm{S}} = P_{1,a}^{\mathrm{S}}$ as $P_{e,\mathrm{X}}^{*,\mathrm{low}}$ attains its minimum at the intersection of $\bar{P}_{e,\mathrm{X}}^*$ and $\hat{P}_{e,\mathrm{X}}^*$.
2) $0 \leq P_{1,b}^{\mathrm{S}} \leq P_{1,a}^{\mathrm{S}}$: in this case, $P_{1,\mathrm{opt}}^{\mathrm{S}} = P_{1,b}^{\mathrm{S}}$ since $P_{e,\mathrm{X}}^{*,\mathrm{low}}$ attains its minimum at $\hat{P}_{e,\mathrm{X}}^*$, evaluated with $P_1^{\mathrm{S}} = P_{1,b}^{\mathrm{S}}$.

Combining the two cases, the optimal allocated power for the SU symbol is $P_{1,\mathrm{opt}}^{\mathrm{S}}$ as given in (30). The minimum value of $P_{e,\mathrm{X}}^{*,\mathrm{low}}$ is $\hat{P}_{e,\mathrm{X}}^*$, evaluated at $P_1^{\mathrm{S}} = P_{1,\mathrm{opt}}^{\mathrm{S}}$. Thus, $P_{e,\mathrm{X},\min}^{*,\mathrm{low}}$ is given as in (29). ∎

*2) SER Performance at* X *in CSS Scenario 2:* Demodulating the PU symbol at X in Rule $R_3$ is as same as the demodulating the PU symbol at D. Similar to the analysis in V-A2, the PU symbol is correctly demodulated at node X if $\tilde{y}_{\mathrm{X}} \in \mathcal{E}_0$. The following proposition is applicable.

**Proposition 4.** *Given $x_{0,n}$ as the composite transmitted symbol at* R*,* X *determines $\tilde{S}_{\dot{m}}$ as the PU's transmitted symbol if*

$$\tilde{z}_{\mathrm{X}} \in \mathcal{E}_{\dot{m},n}, \tag{33}$$

*where $\mathcal{E}_{\dot{m},n} = \{(\tilde{z}_{\mathrm{X},R}, \tilde{z}_{\mathrm{X},I}) \,|\, A_{\dot{m},n}\}$ and $A_{\dot{m},n}$ is defined in the equation (34).*

*Proof:* Denote $\mathcal{E}_{\dot{m}}$ as the detection region of the estimated symbol $\tilde{S}_{\dot{m}}$. This region is bounded by the two rays, $Ov_{\dot{m}}^+$ and $Ov_{\dot{m}}^-$, as shown in Fig. 3. Mathematically , $\mathcal{E}_{\dot{m}}$ is defined as

$$\mathcal{E}_{\dot{m}} = \{U \,|D_{\dot{m}}\}, \tag{35}$$

where $D_{\dot{m}}$ is the condition defined and shown in (36) at the top of next page. $G_1$, $G_2$ are also defined in (36).

Note that $\cos\big(-\big(\varphi_{\dot{m}} + \frac{\pi}{M}\big)\big)$ and $\cos\big(-\big(\varphi_{\dot{m}} - \frac{\pi}{M}\big)\big)$ are positive $\forall \dot{m} \in G_1$. In contrast, they are negative $\forall \dot{m} \in G_2$. On the other hand, $\cos\big(-\big(\varphi_{\dot{m}} + \frac{\pi}{M}\big)\big) < 0$ and $\cos\big(-\big(\varphi_{\dot{m}} - \frac{\pi}{M}\big)\big) > 0$ for $\dot{m} = \frac{M}{4}$; $\cos\big(-\big(\varphi_{\dot{m}} + \frac{\pi}{M}\big)\big) > 0$ and $\cos\big(-\big(\varphi_{\dot{m}} - \frac{\pi}{M}\big)\big) < 0$ for $\dot{m} = \frac{3M}{4}$. Thus, $D_{\dot{m}}$ can be written in a general form as follows:

$$\begin{aligned} &D_{\dot{m}} \\ &= \Big(\Im\{U\}\cos\Big(-\Big(\varphi_{\dot{m}} + \frac{\pi}{M}\Big)\Big) \geq \sin\Big(-\Big(\varphi_{\dot{m}} + \frac{\pi}{M}\Big)\Big)\Re\{U\}\Big) \\ &\quad \cap\Big(\Im\{U\}\cos\Big(-\Big(\varphi_{\dot{m}} - \frac{\pi}{M}\Big)\Big) \leq \sin\Big(-\Big(\varphi_{\dot{m}} - \frac{\pi}{M}\Big)\Big)\Re\{U\}\Big), \\ &\qquad\qquad \forall 0 \leq \dot{m} \leq M-1. \end{aligned} \tag{37}$$

Replacing $U$ with $\tilde{y}_{\mathrm{X}}\big(\tilde{S}_0, U_n\big)$ in (36) and expanding this equation to obtain the region defined in (34). This region is then used to estimate symbol $\tilde{S}_{\dot{m}}$, given $x_{0,n}$ as the transmitted symbol. ∎

Denote $\mathcal{Y}_{\dot{n}|n,\dot{m}}$ as the detection region of the symbol $U_{\dot{n}}$, conditioned on $U_n$ being the transmitted symbol and the detection result $\bar{\bar{m}} = \dot{m}$. Likewise, denote $\bar{\mathcal{Y}}_{\dot{n}|n,\dot{m}}$ as the complementary region of $\mathcal{Y}_{\dot{n}|n,\dot{m}}$, referring to the case where X detects the symbol that is different from $U_{\dot{n}}$, conditioned on the transmitted symbol $U_n$ and the detection result $\bar{\bar{m}} = \dot{m}$.

$\bar{\mathcal{Y}}_{n|n,\dot{m}}$ refers to the detection error conditioned on $\bar{\bar{m}} = \dot{m}$ and the transmitted symbol $U_n$. It is expressed as follows:

$$P_{1,\text{opt}}^{\text{S}} = \max\left\{0, \min\left\{ \overbrace{\frac{-\left(\sin^2\frac{\pi}{M}+\sin^2\frac{\pi}{N}\right)+\sqrt{\left(\sin^2\frac{\pi}{M}+\sin^2\frac{\pi}{N}\right)^2+4P_1\left|h_{\text{RX}}\right|^2\sin^2\frac{\pi}{M}\sin^2\frac{\pi}{N}}}{2\left|h_{\text{RX}}\right|^2\sin^2\frac{\pi}{N}}}^{P_{1,a}^{\text{S}}}, \underbrace{\frac{P_1}{1+\gamma_0}-\frac{\gamma_0}{\left|h_{\text{RD}}\right|^2(1+\gamma_0)}}_{P_{1,b}^{\text{S}}} \right\}\right\}. \tag{30}$$

$$A_{\dot{m},n} \triangleq \left( \underbrace{\overbrace{\left(\Im\left\{\tilde{y}_{\text{X}}\left(\tilde{S}_0,U_n\right)\right\}\cos\left(-\left(\varphi_{\dot{m}}+\frac{\pi}{M}\right)\right)\geq\sin\left(-\left(\varphi_{\dot{m}}+\frac{\pi}{M}\right)\right)\Re\left\{\tilde{y}_{\text{X}}\left(\tilde{S}_0,U_n\right)\right\}\right)}^{a_{\dot{m},n}}}_{b_{\dot{m},n}} \right). \tag{34}$$

$$D_{\dot{m}} = \begin{cases} \left(\begin{matrix}\left(\Im\{U\}\geq\tan\left(-\left(\varphi_{\dot{m}}+\frac{\pi}{M}\right)\right)\Re\{U\}\right)\\ \cap\left(\Im\{U\}\leq\tan\left(-\left(\varphi_{\dot{m}}-\frac{\pi}{M}\right)\right)\Re\{U\}\right)\end{matrix}\right), \text{for } \underbrace{\left(0\leq\dot{m}\leq\frac{M}{4}-1\right)\cup\left(\frac{3M}{4}+1\leq\dot{m}\leq M-1\right)}_{G_1} \\ \left(\begin{matrix}\left(\Im\{U\}\leq\tan\left(-\left(\varphi_{\dot{m}}+\frac{\pi}{M}\right)\right)\Re\{U\}\right)\\ \cap\left(\Im\{U\}\geq\tan\left(-\left(\varphi_{\dot{m}}-\frac{\pi}{M}\right)\right)\Re\{U\}\right)\end{matrix}\right), \text{for } \underbrace{\left(\frac{M}{4}+1\leq\dot{m}\leq\frac{3M}{4}-1\right)}_{G_2} \\ \left(\begin{matrix}\left(\Im\{U\}\leq\tan\left(-\left(\varphi_{\dot{m}}+\frac{\pi}{M}\right)\right)\Re\{U\}\right)\\ \cap\left(\Im\{U\}\leq\tan\left(-\left(\varphi_{\dot{m}}-\frac{\pi}{M}\right)\right)\Re\{U\}\right)\end{matrix}\right), \text{for } \dot{m}=\frac{M}{4} \\ \left(\begin{matrix}\left(\Im\{U\}\geq\tan\left(-\left(\varphi_{\dot{m}}+\frac{\pi}{M}\right)\right)\Re\{U\}\right)\\ \cap\left(\Im\{U\}\geq\tan\left(-\left(\varphi_{\dot{m}}-\frac{\pi}{M}\right)\right)\Re\{U\}\right)\end{matrix}\right), \text{for } \dot{m}=\frac{3M}{4} \end{cases} \tag{36}$$

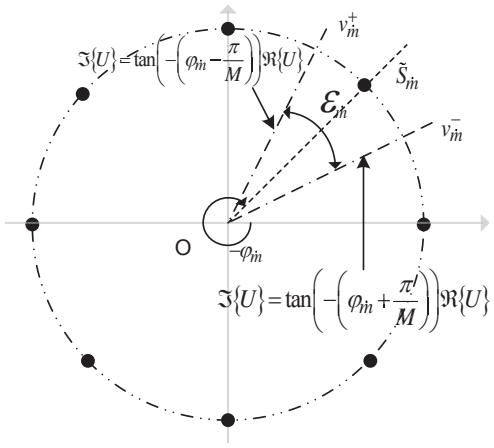


Fig. 3. The detection region $\mathcal{E}_{\dot{m}}$ of the symbol $\tilde{S}_{\dot{m}}$.

$$\bar{\mathcal{Y}}_{n|n,\,\dot{m}} = \left\{\left(\tilde{z}_{\text{X},R},\tilde{z}_{\text{X},I}\right)|C_{0,n,\dot{m}}\right\}, \tag{38}$$

where $C_{0,n,\dot{m}} \triangleq \left(\left|\widehat{y}_{\text{X}}\left(\tilde{S}_0,U_n,\tilde{S}_{\dot{m}}\right)-\sqrt{P_2^{\text{S}}}U_n\right|\geq\frac{d_{\min}}{2}\right)$. Herein, $d_{\min}$, defined as the distance between two nearby points of the PAM constellation, is given by

$$d_{\min} = \sqrt{P_2^{\text{S}}}\left|U_{n+1}-U_n\right| = \frac{2\sqrt{3P_2^{\text{S}}}}{\sqrt{N^2-1}}. \tag{39}$$

Expanding $\widehat{y}_{\text{X}}\left(\tilde{S}_0,U_n,\tilde{S}_{\dot{m}}\right)$ allows us to express $C_{0,n,\dot{m}}$ as

$$C_{0,n,\dot{m}} = \left(c_{\dot{m},n}\cup d_{\dot{m},n}\right), \tag{40}$$

where

$$c_{\dot{m},n} \triangleq \left(\left(\tilde{z}_{\text{X},R}+x_{0,n}\right)\cos\varphi_{\dot{m}}-\tilde{z}_{S_{2,I}}\sin\varphi_{\dot{m}}-x_{0,n}\geq\frac{d_{\min}}{2}\right) \tag{41}$$

and

$$d_{\dot{m},n} \triangleq \left(\left(\tilde{z}_{\text{X},R}+x_{0,n}\right)\cos\varphi_{\dot{m}}-\tilde{z}_{S_{2,I}}\sin\varphi_{\dot{m}}-x_{0,n}\leq-\frac{d_{\min}}{2}\right), \tag{42}$$

The SER $P_{e,\text{X}}^{**}$ which is defined in (21) can be rewritten and computed as follows:

$$\begin{aligned} P_{e,\text{X}}^{**} &= \frac{1}{N}\sum_{n=0}^{N-1}\Pr\left\{\left(\tilde{z}_{\text{X},R},\tilde{z}_{\text{X},I}\right)\in\left(\bigcup_{\dot{m}=0}^{M-1}\left(\bar{\mathcal{Y}}_{n|n,\dot{m}}\cap\mathcal{E}_{\dot{m},n}\right)\right)\right\} \\ &\overset{(a)}{=} \frac{1}{N}\sum_{n=0}^{N-1}\sum_{\dot{m}=0}^{M-1}\underbrace{\Pr\left\{\left(\tilde{z}_{\text{X},R},\tilde{z}_{\text{X},I}\right)\in\left(\bar{\mathcal{Y}}_{n|n,\dot{m}}\cap\mathcal{E}_{\dot{m},n}\right)\right\}}_{P_{e,\text{X},\dot{m},n}^{**}}. \end{aligned} \tag{43}$$

The equality $(a)$ occurs because $\mathcal{E}_{\dot{m},n}$ are the non-overlapping regions for different values of $\dot{m}$. The component $P_{e,\text{X},\dot{m},n}^{**}$ is analytically computed in Appendix A.

We denote $P_2$ to be the total power consumed at R in

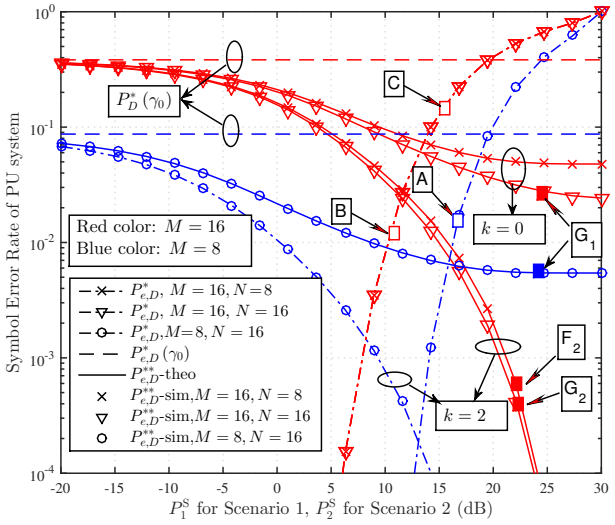


Fig. 4. The SER performance of the PU system against the secondary signal power in Scenario 1 and 2. $P_1 = 30$ dB, $|h_{\mathrm{RD}}| = |h_{\mathrm{RD}}| = 1$, $\gamma_0 = 10$ dB, $(M, N) = (8, 16), (16, 8), (16, 16)$, $k = \{0, 2\}$.

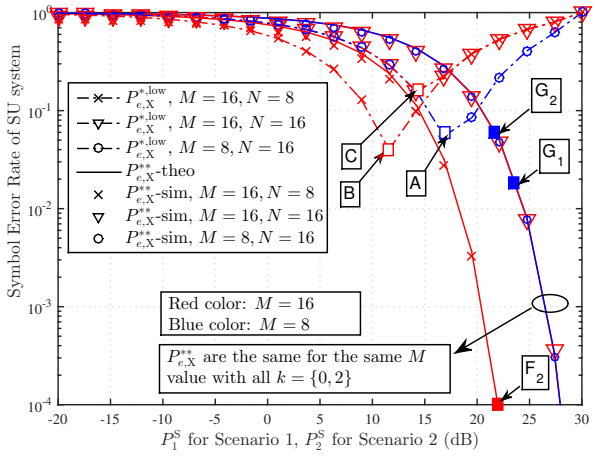


Fig. 5. The SER performance of the SU system against the secondary signal power in Scenario 1 and 2. $P_1 = 30$ dB, $|h_{\mathrm{RD}}| = |h_{\mathrm{RD}}| = 1$, $\gamma_0 = 10$ dB, $(M, N) = (8, 16), (16, 8), (16, 16)$, $k = \{0, 2\}$.

Scenario 2. It is calculated as follows:

$$\begin{aligned} P_2 &= \frac{1}{MN}\sum_{m=0}^{M-1}\sum_{n=0}^{N-1}\left|\sqrt{P_2^{\mathrm{P}}}+\sqrt{t}+\sqrt{P_2^{\mathrm{S}}}U_n\right|^2\left|\tilde{S}_m\right| \\ &= \frac{1}{N}\sum_{n=0}^{N-1}\left|\sqrt{P_2^{\mathrm{P}}}+\sqrt{t}+\sqrt{P_2^{\mathrm{S}}}U_n\right|^2 \\ &\quad+\frac{1}{N}\sum_{n=0}^{N-1}\left(2\sqrt{tP_2^{\mathrm{S}}}+2\sqrt{P_2^{\mathrm{P}}P_2^{\mathrm{S}}}\right)U_n \\ &= P_2^{\mathrm{P}}+t+P_2^{\mathrm{S}}+2\sqrt{P_2^{\mathrm{P}}t}. \end{aligned} \tag{44}$$

As noted in Remark 1, $t$ is set as $t = 3P_2^{\mathrm{S}}\frac{N-1}{N+1} + kP_2^{\mathrm{S}}$. In the simulation section, the effect of $k$ on the SER $P_{e,\mathrm{X},n}^{**}$ and the transmit power $P_2$ will be illustrated in detail.

## VI. Simulation and Discussions

For all simulations, the maximum total power $P_1$ at R is set to be $P_1 = 30$ dB while the noise variance is normalized to 1.

### *A. SER Performances versus the PU and SU Constellation Sizes*

The total power usage at R in CSS Scenario 1 is assumed to be maximum power $P_1$; thus $P_1 = P_1^{\mathrm{S}} + P_1^{\mathrm{P}}$. Meanwhile, the total power usage at R in CSS Scenario 2, known as $P_2$, is limited to be $P_2 \leq P_1$. Thus, CSS Scenario 2 is stricter than that for Scenario 1 in terms of power usage at node R. Another aspect for comparing the two scenarios is the lower-bound SER of the SU system, $P_{e,\mathrm{X}}^{*,\mathrm{low}}$, in Scenario 1.

The simulations in this subsection are obtained the following parameters: $P_1 = 30$ dB, $|h_{\mathrm{RD}}| = |h_{\mathrm{RX}}| = 1$, $M = 16$, $\gamma_0 = 10$ dB, $(M, N) = (8, 16), (16, 8), (16, 16)$. The phase values of $h_{\mathrm{RD}}$ and $h_{\mathrm{RX}}$ do not impact the SER performances.[4] Therefore, we can arbitrarily set any phase values of $h_{\mathrm{RD}}$ and $h_{\mathrm{RX}}$ to perform the simulation. Scenario 2 prioritizes to initiate $P_2^{\mathrm{P}}$ to be $P_2^{\mathrm{P}} = \frac{\gamma_0}{|h_{\mathrm{RD}}|^2}$ as mentioned in Section IV. In this case, $P_2^{\mathrm{P}} = \gamma_0 = 10$ dB because $|h_{\mathrm{RX}}| = 1$, satisfying that $P_2^{\mathrm{P}} < P_1$.

Figs. 4, 5 and 6 display the simulation results in this subsection. The SER performances of the PU and SU systems are illustrated in Fig. 4 and 5, respectively, while the total power usage at R against the secondary SER performance is demonstrated in Fig. 6. It is observed in all three figures that the analytical results on the SER performances in CSS Scenario 2 perfectly match with the corresponding numerical results.

The points $A$, $B$ and $C$ shown in Figs. 4, 5 and 6 corresponds to the case when $P_{e,\mathrm{X},\min}^{*,\mathrm{low}}$ w.r.t different constellation size pairs $(M, N) = (8, 16), (16, 8), (16, 16)$. The determination of these points is shown in Fig. 5. The points $G_1$, $G_2$ and $F_2$ as seen in Figs. 4, 5 and 6 indicate the lowest $P_{e,\mathrm{X}}^{**}$ according to the cases $(N, k) = (16, 0), (16, 2)$ and $(8, 2)$ in Scenario 2, respectively. The lowest $P_{e,\mathrm{X}}^{**}$ w.r.t $(N, k) = (8, 0)$ is is too small for displaying in Figs. 4, 5 and 6. These points, $G_1$, $G_2$, $F_2$ are determined when $P_2 = P_1$, implying that the increase in $P_2^{\mathrm{S}}$ causes the total power $P_2$ to reach its limit as shown in Fig. 6.

It can be seen in Fig. 4 that all graphs of $P_{e,\mathrm{D}}^{**}$ is below the value $P_{e,\mathrm{D}}(\gamma_0)$, as affirmed by Proposition 1. Here, the coefficient $k$ represents amount of additional power $kP_2^{\mathrm{S}}$ used in $t$ in addition to the regular power amount, $3P_2^{\mathrm{S}}\frac{N-1}{N+1}$. This coefficient plays an important role in PU's SER performance

[4]It is because noises at receivers are complex Gaussian noise. This can be checked via simulation with various random specific phase values of $h_{\mathrm{RD}}$ and $h_{\mathrm{RX}}$.

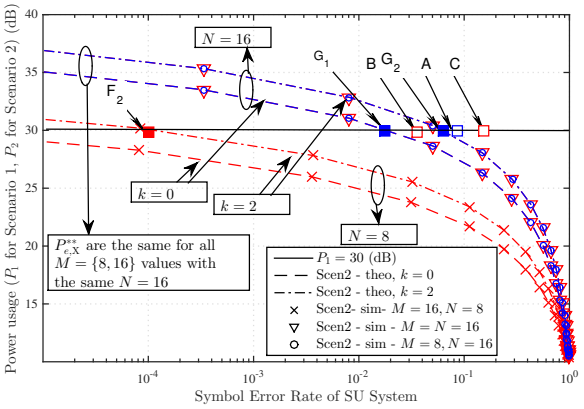


Fig. 6. The total power usage performance of the SU system against the secondary signal power in Scenario 1 and 2. $P_1 = 30$ dB, $|h_{\mathrm{RD}}| = |h_{\mathrm{RD}}| = 1$, $\gamma_0 = 10$ dB, $(M, N) = (8, 16), (16, 8), (16, 16)$, $k = \{0, 2\}$.

in Scenario 2. When $P_2^{\mathrm{S}}$ is sufficiently large, increasing $P_2^{\mathrm{S}}$ no longer decreases $P_{e,\mathrm{D}}^{**}$, even for the case $k = 0$. It can be explained by the value $\gamma_{\mathrm{D},0}$. From (23), it is easily to find that $\gamma_{\mathrm{D},0} = |h_{\mathrm{RD}}|^2 P_2^{\mathrm{P}}$ when $k = 0$. $\gamma_{\mathrm{D},0}$ is independent of $P_2^{\mathrm{S}}$, providing a constant lower-bound of $P_{e,\mathrm{D}}^{**}$ according to (22). Whereas, the other $\gamma_{\mathrm{D},n}$ with $n \neq 0$ are still dependent of $P_2^{\mathrm{S}}$; they approach $+\infty$ as $P_2^{\mathrm{S}}$ increases to $+\infty$. Consequently, $P_{e,\mathrm{D}}^{**}$ approximates to $\frac{1}{N} H_{\mathrm{D}}(\gamma_{\mathrm{D},0})$ when $P_2^{\mathrm{S}}$ is sufficiently large. This refers to the independence of $P_{e,\mathrm{D}}^{**}$ from $P_2^{\mathrm{S}}$ when $P_2^{\mathrm{S}}$ is sufficiently large.

For the case $k = 2$, $P_{e,\mathrm{D}}^{**}$ always decreases with increasing $P_2^{\mathrm{S}}$, *i.e.*, $P_{e,\mathrm{D}}^{**} \to 0$ if $P_2^{\mathrm{S}} \to +\infty$. The additional amount of power $kP_2^{\mathrm{S}}$, for $k > 0$, results in all $\gamma_{\mathrm{D},n}$, including $\gamma_{\mathrm{D},0}$, to be dependent on $P_2^{\mathrm{S}}$. It is easy to see that the component $\sqrt{t} + \sqrt{P_2^{\mathrm{S}}} U_n$ depends on $P_2^{\mathrm{S}}$ for $k > 0$. The larger value of $k$ is, the higher degree of dependence is. Therefore, $\gamma_{\mathrm{D},n}, \forall n$, increases to $+\infty$ as $P_2^{\mathrm{S}}$ increases, making $P_{e,\mathrm{D}}^{**}$ decreasing to 0. It should be noted that the secondary SER graphs of Scenario 2 are the same for both $k = 0$ and $k = 2$ because $t$ does not carry any secondary information.

In most of the current spectrum sharing methodologies, including the CSS Scenario 1, any increase in the secondary signal power typically induce more interference with the PU systems. Thus, the PU system performance will be degraded. For example, the performance of the PU system is getting poorer, as observed in the graph of $P_{e,\mathrm{D}}^{*}$ in Fig. 4. Several other approaches have to employ the high-cost and complexity method, *e.g.*, beamforming solution, to combat with interference [26], [30]. The beamforming technique is impossible in our system configuration because of the use of single relay equipped with single antenna. However, the proposed method in CSS Scenario 2 has overcome these disadvantages. It can be observed that the larger value of $P_2^{\mathrm{S}}$ is used, the lower secondary SER is as a result while $P_{e,\mathrm{D}}^{*}$ is always assured to be below $P_{e,\mathrm{D}}^{**}(\gamma_0)$. Especially, for $k > 0$, both primary and secondary SER performances are improved as result of the increase in $P_2^{\mathrm{S}}$.

Let us further compare the efficiency of both CSS Scenarios 1 and 2. Firstly, it can be easily observed that the proposed method in CSS Scenario 2 always meets the target primary SER value: $P_{e,\mathrm{D}}^{**} \leq P_{e,\mathrm{D}}^{*}(\gamma_0)$. Meanwhile, for the large value of $P_1^{\mathrm{S}}$, *e.g.*, $P_1^{\mathrm{S}} \geq 20$ dB, Scenario 1 does not attain this property. Secondly, for $k = 0$, Scenario 2 always has its lowest values of $P_{e,\mathrm{X}}^{*}$ (w.r.t the points $G_1$ for $(M, N) = (16, 16)$ or $(8, 16)$ in Fig. 5)[5] to be always much lower than $P_{e,\mathrm{X,min}}^{*,\mathrm{low}}$ (as compared to those w.r.t the points $A$ or $C$ in the same figure, respectively). Thirdly, for $k = 2$, it is obvious that the lowest $P_{e,\mathrm{X}}^{**}$ values (w.r.t $G_2$ if $N = 16$, $F_2$ w.r.t $N = 8$) will be larger than those with $k = 0$. However, we can see that $k = 2$ still produces the $P_{e,\mathrm{X}}^{**}$ which is much lower than $P_{e,\mathrm{X,min}}^{*,\mathrm{low}}$ when $N = 8$ (point $F_2$ compared to $B$ in Fig. 5). This can be generalized that we can find a certain value $k$ where $k > 0$ that benefits $P_{e,\mathrm{D}}^{**}$ and the increase of $P_2^{\mathrm{S}}$ helps the proposed method obtain the better secondary SER performance as compared to the conventional. Finally, as a result of the third advantage, the proposed method can use less power at R to achieve a superior performance, compared to Scenario 1. We can see that in Scenario 1, at point $B$, which is corresponding to $P_{e,\mathrm{X,min}}^{*,\mathrm{low}}$ for $N = 8$, $P_1^{\mathrm{S}}$ is $P_1^{\mathrm{S}} \approx 10$ dB. For the graphs with $N = 8$ in Scenario 2, at $P_2^{\mathrm{S}} = 20$ dB, we attain $P_{e,\mathrm{D}}^{**}\big|_{P_2^{\mathrm{S}}=20\mathrm{dB}} < P_{e,\mathrm{D}}^{*}\big|_{P_1^{\mathrm{S}}=10\mathrm{dB}} \leq P_{e,\mathrm{D}}^{*}(\gamma_0)$, $P_{e,\mathrm{X}}^{**}\big|_{P_2^{\mathrm{S}}=20\mathrm{dB}} < P_{e,\mathrm{X,min}}^{*,\mathrm{low}}\big|_{P_1^{\mathrm{S}}=10\mathrm{dB}}$ and $P_2 < P_1$.

### *B. SER versus Target SINR $\gamma_0$ at* D

In Scenario 1, the co-existing system is set to operate at point which $P_{e,\mathrm{X,min}}^{**,\mathrm{low}}$ occurs. This can be easily to determine by setting $P_1^{\mathrm{S}} = P_{1,\mathrm{opt}}^{\mathrm{S}}$, as being shown in (30). $P_1^{\mathrm{P}}$ is then determined by $P_1^{\mathrm{P}} = P_1 - P_{1,\mathrm{opt}}^{\mathrm{S}}$. The power usage at R is set to be $P_1$ for both scenarios. In Scenario 2, $P_2^{\mathrm{P}}$ is set as follows: $P_2^{\mathrm{P}} = \min\left\{\frac{\gamma_0}{|h_{\mathrm{RD}}|^2}, P_1\right\}$, to attain the setting as mentioned in Section IV as well as limiting $P_2^{\mathrm{P}}$ to be $P_2^{\mathrm{P}} \leq P_1$. According to Equation (44), the allocated power for the SU's symbol $P_2^{\mathrm{S}}$ is determined as the solution of the following equation:

$$(a+1)P_2^{\mathrm{S}} + 2\sqrt{aP_2^{\mathrm{P}}P_2^{\mathrm{S}}} + P_2^{\mathrm{P}} - P_1 = 0, \qquad (45)$$

where $a = 3\frac{N-1}{N+1} + k$. Resolving this quadratic equation yields the following root:

$$P_2^{\mathrm{S}} = \left(\frac{-\sqrt{aP_2^{\mathrm{P}}} + \sqrt{(a+1)P_1 - P_2^{\mathrm{P}}}}{a+1}\right)^2. \qquad (46)$$

It is obvious that $0 \leq P_2^{\mathrm{S}} \leq P_1$, $0 \leq P_2^{\mathrm{P}} \leq P_1$ and $P_2 = P_1$ are always satisfied. Therefore, R consumes the same power $P_1$ in this circumstance.

Figs. 7 presents the result on the PU's SER performance versus the target SINR $\gamma_0$. Here, $P_1$ is still 30 dB, $M = 16$,

[5]It should be noted that the lowest values of $P_{e,\mathrm{X}}^{**}$ are defined to be secondary SER value when $P_2 = P_1$. This definition validates the fairness in term of the power consumption at R while performing the comparison.

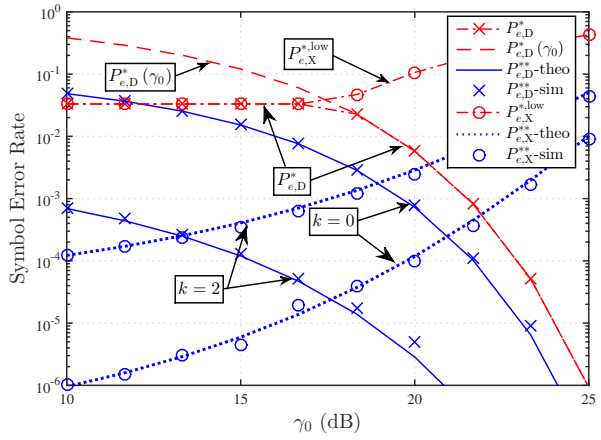


Fig. 7. The SER of the PU system against the changes of $\gamma_0$. The other parameters are set as follows: $P_1^{\mathrm{S}}$, $P_1^{\mathrm{P}}$, $P_2^{\mathrm{P}}$ and $P_2^{\mathrm{S}}$ are set as described in Subsection VI-B. $P_1 = 30$ dB, $|h_{\mathrm{RD}}|^2 = |h_{\mathrm{RX}}| = 1$, $k = \{0, 2\}$, $M = 16$, $N = 8$.

$N = 8$, $|h_{\mathrm{RD}}| = |h_{\mathrm{RX}}| = 1$. The settings of $P_1^{\mathrm{S}}$, $P_1^{\mathrm{P}}$, $P_2^{\mathrm{P}}$ and $P_2^{\mathrm{S}}$ are the same as the results presented in the above paragraph. It is observed that the performances $P^{**}_{e,\mathrm{D}}$ and $P^{**}_{e,\mathrm{X}}$ are comparable to their counterparts $P^{*}_{e,\mathrm{D}}$ and $P^{*,\mathrm{low}}_{e,\mathrm{X,min}}$.

### C. Future work

The study in this paper can be extended to various modulation types, *e.g.*, *M*-ary QAM. Therefore, the finding for the lowest SER lower-bound (as similar to $P^{**,\mathrm{low}}_{e,\mathrm{X,min}}$) typically can be considered as the near-future discussions.

Fig. 4 shows that $k > 0$ can be used to adjust the performance of $P^{**}_{e,\mathrm{D}}$ to meet the a certain target of the $P^{*}_{e,\mathrm{D}}$ value, including $P^{*}_{e,\mathrm{D}}(\gamma_0)$. Therefore, the condition that $t \geq 3P_2^{\mathrm{S}}\frac{N-1}{N+1}$ as mentioned in Proposition 1 is not mandatory, leading to possible reduction in the power usage at R. The performance of $P^{**}_{e,\mathrm{D}}$ is also much improved for the large values of $|h_{\mathrm{RD}}|$ when $k > 0$. Consequently, $k$ can be adjusted accordingly to the channel quality so that any targets of the primary and secondary SER performances can be satisfied.

This study shows an example that modulation features can be exploited as a dimension to provide the sharing spectrum in which the secondary system does not cause any interference with the primary receiver. Thus, it will be interesting for further research to investigate the combination of the proposed method and exploitation of the T/F/S spectrum holes.

## VII. Conclusion

This article proposes the concept of cooperative modulation when performing the cooperative spectrum sharing at a given time/frequency/spatial coordinate, known as the cooperative modulation-based spectrum sharing. The M-PSK property of the PU signal is proved that it can be treated as a dimension to exploit spectrum holes. The sharing spectrum space created by the proposed method has advantages as follow. First, not only does the secondary spectrum access not cause interference but also improve the SER performance at the primary receiver. Second, the PU system is not required to do much self-configuration for spectrum sharing since its detection mechanism is the same as the case without spectrum sharing. The study also found the exact SER expression for the proposed method and strictly compared the performance with the conventional method. The outcome of the comparison shows that the proposed method is better than the conventional one.

## Appendix A
## Calculate $P^{**}_{e,\mathrm{X},\dot{m},n}$

$A_{\dot{m},n}$ is defined as given in expression (34). The two component events, $a_{\dot{m},n}$ and $b_{\dot{m},n}$, can be expanded and rewritten as shown in the expressions (47) where $X_{\dot{m}} \triangleq \tilde{z}_{\mathrm{X},R}\sin\varphi_{\dot{m}} + \tilde{z}_{\mathrm{X},I}\cos\varphi_{\dot{m}}$ and $Y_{\dot{m}} \triangleq \tilde{z}_{\mathrm{X},R}\cos\varphi_{\dot{m}} - \tilde{z}_{\mathrm{X},I}\sin\varphi_{\dot{m}}$. It should be noted that $\sin\frac{\pi}{M}$ and $\cos\frac{\pi}{M}$ are always positive while performing this expansion, because $M \geq 4$ is assumed in this study. It can be easily examined that $E\{X_{\dot{m}}Y_{\dot{m}}\} = 0$, leading to the result that $X_{\dot{m}}$ and $Y_{\dot{m}}$ are the two independently identically distributed Gaussian random variables with zero mean and variance $\frac{\sigma^2_{\mathrm{X}}}{2} = \frac{1}{2|h_{\mathrm{RX}}|^2}$.

The components can be rewritten as follows: Define the following 4 events, $a_{\dot{m},n}$, $b_{\dot{m},n}$ as given in (47) and $c_{\dot{m},n}$, $d_{\dot{m},n}$ as given next.

$$c_{\dot{m},n} = \left(\underbrace{\mathcal{Y}_{\dot{m}} \geq \frac{d_{\min}}{2} + (1-\cos\varphi_{\dot{m}})\,x_{0,n}}_{\mu_{1,\dot{m},n}}\right), \tag{48}$$

$$d_{\dot{m},n} = \left(\underbrace{\mathcal{Y}_{\dot{m}} \leq -\frac{d_{\min}}{2} + (1-\cos\varphi_{\dot{m}})\,x_{0,n}}_{\mu_{2,\dot{m},n}}\right). \tag{49}$$

It is clear that $P^{**}_{e,S_{2,\dot{m},n}}$ can be rewritten as follows:

$$\begin{aligned} P^{**}_{e,S_{2,\dot{m},n}} &= \Pr\{(a_{\dot{m},n}\cap b_{\dot{m},n})\cap(c_{\dot{m},n}\cup d_{\dot{m},n})\} \\ &= \Pr\left\{\underbrace{(a_{\dot{m},n}\cap b_{\dot{m},n}\cap c_{\dot{m},n})}_{T_{1,\dot{m},n}} \cup \underbrace{(a_{\dot{m},n}\cap b_{\dot{m},n}\cap d_{\dot{m},n})}_{T_{2,\dot{m},n}}\right\} \\ &= \Pr\{T_{1,\dot{m},n}\} + \Pr\{T_{2,\dot{m},n}\}. \end{aligned} \tag{50}$$

Our focus is now to calculate $\Pr\{T_{1,\dot{m},n}\}$ and $\Pr\{T_{2,\dot{m},n}\}$.

### A. Calculate $\Pr\{T_{1,\dot{m},n}\}$

We define $\Delta_1, \Delta_2, \Delta_3$ to be the events as respectively described as follows:

$$\begin{aligned} &\Delta_1 \triangleq \left(\mu_{1,\dot{m},n} \geq \max\{\delta_{1,\dot{m},n}(X_{\dot{m}}), \delta_{2,\dot{m},n}(X_{\dot{m}})\}\right) \\ \Rightarrow\ &\Delta_1 = \left(r_{2,\dot{m},n} \leq X_{\dot{m}} \leq r_{1,\dot{m},n}\right) \end{aligned} \tag{51}$$

$$\begin{aligned} &\Delta_2 \triangleq \left(\delta_{2,\dot{m},n}(X_{\dot{m}}) \geq \max\{\delta_{1,\dot{m},n}(X_{\dot{m}}), \mu_{1,\dot{m},n}\}\right) \\ \Rightarrow\ &\Delta_2 = \left(X_{\dot{m}} \geq r_{3,\dot{m},n}\right) \end{aligned} \tag{52}$$

$$\begin{aligned} &\Delta_3 \triangleq \left(\delta_{1,\dot{m},n}(X_{\dot{m}}) \geq \max\{\delta_{2,\dot{m},n}(X_{\dot{m}}), \mu_{1,\dot{m},n}\}\right) \\ \Rightarrow\ &\Delta_3 = \left(X_{\dot{m}} \leq r_{4,\dot{m},n}\right) \end{aligned} \tag{53}$$

$$a_{\dot{m},n} = \left(X_{\dot{m}} \cos\tfrac{\pi}{M} + Y_{\dot{m}} \sin\tfrac{\pi}{M} \geq -x_{0,n} \sin\left(\varphi_{\dot{m}} + \tfrac{\pi}{M}\right)\right) = \left(Y_{\dot{m}} \geq \underbrace{\frac{-x_{0,n}\sin\left(\varphi_{\dot{m}} + \frac{\pi}{M}\right) - X_{\dot{m}}\cos\frac{\pi}{M}}{\sin\left(\pi/M\right)}}_{\delta_{1,\dot{m},n}(X_{\dot{m}})}\right),$$
$$b_{\dot{m},n} = \left(X_{\dot{m}} \cos\tfrac{\pi}{M} - Y_{\dot{m}} \sin\tfrac{\pi}{M} \leq -x_{0,n} \sin\left(\varphi_{\dot{m}} - \tfrac{\pi}{M}\right)\right) = \left(Y_{\dot{m}} \geq \underbrace{\frac{x_{0,n}\sin\left(\varphi_{\dot{m}} - \frac{\pi}{M}\right) + X_{\dot{m}}\cos\frac{\pi}{M}}{\sin\left(\pi/M\right)}}_{\delta_{2,\dot{m},n}(X_{\dot{m}})}\right) \quad (47)$$

where $\delta_{1,\dot{m},n}\left(X_{\dot{m}}\right)$ and $\delta_{2,\dot{m},n}\left(X_{\dot{m}}\right)$ are defined in the equation (47). $r_{1,\dot{m},n}$, $r_{2,\dot{m},n}$, $r_{3,\dot{m},n}$ and $r_{4,\dot{m},n}$ are determined as follows:

$$r_{1,\dot{m},n} = \tan\left(\frac{\pi}{M}\right)\left(\mu_{1,\dot{m},n} - \frac{x_{0,n}\sin\left(\varphi_{\dot{m}} - (\pi/M)\right)}{\sin\left(\pi/M\right)}\right), \quad (54)$$

$$r_{2,\dot{m},n} = -\tan\left(\frac{\pi}{M}\right)\left(\mu_{1,\dot{m},n} + \frac{x_{0,n}\sin(\varphi_{\dot{m}} + (\pi/M))}{\sin(\pi/M)}\right), \quad (55)$$

$r_{3,\dot{m},n} = \max\left\{r_{5,\dot{m},n}, r_{1,\dot{m},n}\right\}$, $r_{4,\dot{m},n} = \min\left\{r_{5,\dot{m},n}, r_{2,\dot{m},n}\right\}$ and $r_{5,\dot{m},n} = -x_{0,n}\sin\varphi_{\dot{m}}$.

We define probability functions $F_1\left(\alpha,\beta,\gamma\right)$ and $F_2\left(\alpha,\beta,\gamma,\varepsilon\right)$ as given in Appendix B. Applying the computation result in Appendix B, the probabilities $\Pr\left\{T_{1,\dot{m},n} \cap \Delta_1\right\}$, $\Pr\left\{T_{1,\dot{m},n} \cap \Delta_2\right\}$ and $\Pr\left\{T_{1,\dot{m},n} \cap \Delta_3\right\}$ are computed as follows:

$$\Pr\left\{T_{1,\dot{m},n} \cap \Delta_1\right\} = \int_{r_{2,\dot{m},n}}^{r_{1,\dot{m},n}} \Pr\{Y_{\dot{m}} \geq \mu_{1,\dot{m},n}\} p_{X_{\dot{m}}}(v)\, dv = F_1\left(\mu_{1,\dot{m},n}, r_{2,\dot{m},n}, r_{1,\dot{m},n}\right), \quad (56)$$

$$\Pr\{T_{1,\dot{m},n} \cap \Delta_2\} = \int_{r_{3,\dot{m},n}}^{+\infty} \Pr\{Y_{\dot{m}} \geq \delta_{2,\dot{m},n}(v)\} p_{X_{\dot{m}}}(v)\, dv = F_2\left(\cot\frac{\pi}{M}, r_{3,\dot{m},n}, +\infty, \frac{x_{0,n}\sin\left(\varphi_{\dot{m}} - (\pi/M)\right)}{\cos\left(\pi/M\right)}\right), \quad (57)$$

$$\Pr\left\{T_{1,\dot{m},n} \cap \Delta_3\right\} = \int_{-\infty}^{r_{4,\dot{m},n}} \Pr\{Y_{\dot{m}} \geq \delta_{1,\dot{m},n}(v)\}\, p_{X_{\dot{m}}}(v) dv = F_2\left(-\cot\frac{\pi}{M}, -\infty, r_{4,\dot{m},n}, \frac{x_{0,n}\sin(\varphi_{\dot{m}} + (\pi/M))}{\cos\left(\pi/M\right)}\right). \quad (58)$$

The probability $\Pr\left\{T_{1,\dot{m},n}\right\}$ is determined as follows:

$$\Pr\left\{T_{1,\dot{m},n}\right\} = \Pr\left\{T_{1,\dot{m},n} \cap \left(\Delta_1 \cup \Delta_2 \cup \Delta_3\right)\right\} \overset{(a)}{=} \Pr\left\{T_{1,\dot{m},n} \cap \Delta_1\right\} + \Pr\left\{T_{1,\dot{m},n} \cap \Delta_2\right\} + \Pr\left\{T_{1,\dot{m},n} \cap \Delta_3\right\}. \quad (59)$$

The equality (a) in the above expression occurs because all $\Delta_1$, $\Delta_2$ and $\Delta_3$ determine the three non-overlapping regions of the random variable $X_{\dot{m}}$ and $Y_{\dot{m}}$, respectively; these regions create the entire space of $X_{\dot{m}}$ and $Y_{\dot{m}}$.

### *B. Calculate* $\Pr\left\{T_{2,\dot{m},n}\right\}$

$\Pr\left\{T_{2,\dot{m},n}\right\}$ can be rewritten as follows:

$$\Pr\{T_{2,\dot{m},n}\} = \Pr\{\underbrace{a_{\dot{m},n} \cap b_{\dot{m},n}}_{T^{**}_{2,\dot{m},n}}\} - \Pr\{\underbrace{a_{\dot{m},n} \cap b_{\dot{m},n} \cap \bar{d}_{\dot{m},n}}_{T^{*}_{2,\dot{m},n}}\} \quad (60)$$

where $\bar{d}_{\dot{m},n}$ is the complementary event of $d_{\dot{m},n}$, $\bar{d}_{\dot{m},n} = (Y_{\dot{m}} \geq \mu_{2,\dot{m},n})$. Let $\Delta_4$ and $\Delta_5$ denote the events

$$\Delta_4 \triangleq \left(\delta_{1,\dot{m},n}\left(X_{\dot{m}}\right) \leq \delta_{2,\dot{m},n}\left(X_{\dot{m}}\right)\right) \Rightarrow \Delta_4 = \left(X_{\dot{m}} \geq r_{5,\dot{m},n}\right) \quad (61)$$

$$\Delta_5 \triangleq \left(\delta_{1,\dot{m},n}\left(X_{\dot{m}}\right) \geq \delta_{2,\dot{m},n}\left(X_{\dot{m}}\right)\right) \Rightarrow \Delta_5 = \left(X_{\dot{m}} \leq r_{5,\dot{m},n}\right). \quad (62)$$

Therefore,

$$\Pr\left\{T^{**}_{2,\dot{m},n} \cap \Delta_4\right\} = \int_{r_{5,\dot{m},n}}^{+\infty} \Pr\{Y_{\dot{m}} \geq \delta_{2,\dot{m},n}(v)\} p_{X_{\dot{m}}}(v)\, dv = F_2\left(\cot\frac{\pi}{M}, r_{5,\dot{m},n}, +\infty, \frac{x_{0,n}\sin\left(\varphi_{\dot{m}} - (\pi/M)\right)}{\cos\left(\pi/M\right)}\right) \quad (63)$$

$$\Pr\left\{T^{**}_{2,\dot{m},n} \cap \Delta_5\right\} = \int_{-\infty}^{r_{5,\dot{m},n}} \Pr\{Y_{\dot{m}} \geq \delta_{1,\dot{m},n}\left(v\right)\} p_{X_{\dot{m}}}(v)\, dv = F_2\left(-\cot\frac{\pi}{M}, -\infty, r_{5,\dot{m},n}, \frac{x_{0,n}\sin\left(\varphi_{\dot{m}} + (\pi/M)\right)}{\cos\left(\pi/M\right)}\right) \quad (64)$$

$\Pr\left\{T^{**}_{2,\dot{m},n}\right\}$ is calculated as a result of

$$\Pr\left\{T^{**}_{2,\dot{m},n}\right\} = \Pr\left\{T^{**}_{2,\dot{m},n} \cap \Delta_4\right\} + \Pr\left\{T^{**}_{2,\dot{m},n} \cap \Delta_5\right\} \quad (65)$$

The probability $\Pr\left\{T^{*}_{2,\dot{m},n}\right\}$ can be calculated as similar to the computation for $\Pr\left\{T_{1,\dot{m},n}\right\}$. Therefore, it can be expressed as follows:

$$\Pr\left\{T^{*}_{2,\dot{m},n}\right\} = F_1\left(\mu_{2,\dot{m},n}, \dot{r}_{2,\dot{m},n}, \dot{r}_{1,\dot{m},n}\right) + F_2\left(\cot\frac{\pi}{M}, \dot{r}_{3,\dot{m},n}, +\infty, \frac{x_{0,n}\sin\left(\varphi_{\dot{m}} - (\pi/M)\right)}{\cos\left(\pi/M\right)}\right) + F_2\left(-\cot\frac{\pi}{M}, -\infty, \dot{r}_{4,\dot{m},n}, \frac{x_{0,n}\sin\left(\varphi_{\dot{m}} + (\pi/M)\right)}{\cos\left(\pi/M\right)}\right) \quad (66)$$

where $r_{3,\dot{m},n} = \max\left\{r_{5,\dot{m},n}, \dot{r}_{1,\dot{m},n}\right\}$ and $r_{4,\dot{m},n} = \min\left\{r_{5,\dot{m},n}, \dot{r}_{2,\dot{m},n}\right\}$,

$$\dot{r}_{1,\dot{m},n} = \tan\left(\frac{\pi}{M}\right)\left(\mu_{2,\dot{m},n} - \frac{x_{0,n}\sin\left(\varphi_{\dot{m}} - (\pi/M)\right)}{\sin\left(\pi/M\right)}\right), \quad (67)$$

$$\dot{r}_{2,\dot{m},n} = -\tan\left(\frac{\pi}{M}\right)\left(\mu_{2,\dot{m},n} + \frac{x_{0,n}\sin\left(\varphi_{\dot{m}} + (\pi/M)\right)}{\sin\left(\pi/M\right)}\right) \quad (68)$$

## APPENDIX B
## DEFINING AND CALCULATING $F_1(\alpha,\beta,\gamma)$ AND $F_2(\alpha,\beta,\gamma,\epsilon)$

Given $X_{\dot{m}}$ and $Y_{\dot{m}}$ as the two random variables defined in Appendix A, denote $F_1(\alpha,\beta,\gamma)$as the probability function

$$F_1(\alpha,\beta,\gamma) \triangleq \Pr\{Y_{\dot{m}} \geq \alpha, \beta \leq X_{\dot{m}} \leq \gamma\}, \quad (69)$$

The calculation of $F_1(\alpha,\beta,\gamma)$ is as follows:

$$F_1(\alpha,\beta,\gamma) = 0, \forall \beta > \gamma, \quad (70)$$

and

$$\begin{aligned} F_1(\alpha,\beta,\gamma) &= \Pr\{Y_{\dot{m}} \geq \alpha\} \Pr\{\beta \leq X_{\dot{m}} \leq \gamma\} \\ &= Q\left(\frac{\alpha\sqrt{2}}{\sigma_{\mathrm{X}}}\right)\left[Q\left(\frac{\beta\sqrt{2}}{\sigma_{\mathrm{X}}}\right) - Q\left(\frac{\gamma\sqrt{2}}{\sigma_{\mathrm{X}}}\right)\right], \\ &\qquad \forall \beta \leq \gamma. \end{aligned} \quad (71)$$

Denote $F_2(\alpha,\beta,\gamma,\varepsilon)$ as the probability function

$$F_2(\alpha,\beta,\gamma,\varepsilon) \triangleq \Pr\{Y_{\dot{m}} \geq \alpha(\varepsilon + X_{\dot{m}}), \beta \leq X_{\dot{m}} \leq \gamma\}. \quad (72)$$

This function is calculated in multiple steps as given in (76)–(80) in the following page. In that process, we need to calculate two functions $\phi(\alpha,\beta,\gamma,\varepsilon)$ and $\varphi(\alpha,\beta,\gamma,\varepsilon)$ as follows.

Let $\phi(\alpha,\beta,\gamma,\varepsilon)$ be the probability function

$$\begin{aligned} \phi(\alpha,\beta,\gamma,\varepsilon) &\triangleq \int_{\beta}^{\gamma} \exp\left(-\alpha^2\frac{(\varepsilon+v)^2}{\sigma_{\mathrm{X}}^2}\right)\frac{1}{\sigma_{\mathrm{X}}\sqrt{\pi}}\exp\left(-\frac{v^2}{\sigma_{\mathrm{X}}^2}\right)dv \\ &= \frac{1}{\sqrt{1+a^2}}\exp\left(-\frac{\alpha^2\varepsilon^2}{(1+\alpha^2)\sigma_{\mathrm{X}}^2}\right) \\ &\quad \times\left[Q\left(\frac{\sqrt{2}}{\sigma_{\mathrm{X}}}\left(\frac{\alpha^2}{\sqrt{1+\alpha^2}}\varepsilon + \beta\sqrt{1+\alpha^2}\right)\right)\right. \\ &\quad \left. -Q\left(\frac{\sqrt{2}}{\sigma_{\mathrm{X}}}\left(\frac{\alpha^2}{\sqrt{1+\alpha^2}}\varepsilon + \gamma\sqrt{1+\alpha^2}\right)\right)\right]. \end{aligned} \quad (73)$$

Let $\varphi(\alpha,\beta,\gamma,\varepsilon)$ be the probability function

$$\varphi(\alpha,\beta,\gamma,\varepsilon) \triangleq \frac{1}{\pi}\int_0^{\pi/2}\int_{\beta}^{\gamma}\exp\left(-\frac{\alpha^2(\varepsilon+v)^2}{\sigma_{\mathrm{X}}^2\sin^2\theta}\right)p_V(v)\,dvd\theta \quad (74)$$

where $V$ is the real Gaussian random variable with zero mean and variance $\sigma_{\mathrm{X}}^2/2$; $p_V(v) = \frac{1}{\sigma_{\mathrm{X}}\sqrt{\pi}}\exp\left(-\frac{v^2}{\sigma_{\mathrm{X}}^2}\right)$ is the PDF function of $V$. According to the expression (73), $\varphi(\alpha,\beta,\gamma,\varepsilon)$ can be computed as follows:

$$\begin{aligned} \varphi(\alpha,\beta,\gamma,\varepsilon) &= \frac{1}{\pi}\int_0^{\pi/2}\phi\left(\frac{\alpha}{\sin\theta},\beta,\gamma,\varepsilon\right)d\theta \\ &\overset{(a)}{=} \frac{1}{2L}\sum_{l=1}^{L}\phi\left(\frac{\alpha}{\sin\theta_l},\beta,\gamma,\varepsilon\right), \end{aligned} \quad (75)$$

where $\theta_0 = 0$ and $\theta_l = l\frac{\pi}{2L}$. The approximation $(a)$ can be attained with a sufficiently large and finite value of $L$. $L = 20$ is used in this paper. It can be easily observed that $\varphi(\alpha,\beta,\gamma,\varepsilon) = \varphi(-\alpha,\beta,\gamma,\varepsilon)$.

## REFERENCES


[1] Q. Zhao and B. M. Sadler, "A survey of dynamic spectrum access," *IEEE Signal Process. Mag.*, vol. 24, no. 3, pp. 79–89, 2007.

[2] T. Duong, D. da Costa, T. Tsiftsis, C. Zhong, and A. Nallanathan, "Outage and diversity of cognitive relaying systems under spectrum sharing environments in Nakagami-m fading," *IEEE Commun. Letters*, vol. 15, no. 12, pp. 2075–2078, Dec. 2012.

[3] K. J. Kim, T. Q. Duong, and N. Tran, "Performance analysis of cognitive spectrum-sharing single-carrier systems with relay selection," *IEEE Trans. Signal Proc.*, vol. 60, no. 12, pp. 6435–6449, Dec. 2012.

[4] M. Xia and S. Aissa, "Cooperative af relaying in spectrum-sharing systems: Performance analysis under average interference power constraints and Nakagami-m fading," *IEEE Trans. Commun.*, vol. 60, no. 6, pp. 1523–1533, Jun. 2012.

[5] M. Xia and S. Aissa, "Cooperative AF relaying in spectrum-sharing systems: Outage probability analysis under co-channel interferences and relay selection," *IEEE Trans. Commun.*, vol. 60, no. 11, pp. 3252–3262, Nov. 2012.

[6] Z. Wang and W. Zhang, "Exploiting multiuser diversity with 1-bit feedback for spectrum sharing," *IEEE Trans. Commun.*, vol. 62, no. 1, pp. 29–40, Jan. 2014.

[7] E. E. Benitez Olivo, D. P. Moya Osorio, D. B. da Costa, and J. C. Silveira Santos Filho, "Outage performance of spectrally efficient schemes for multiuser cognitive relaying networks with underlay spectrum sharing," *IEEE Trans. Wireless Commun.*, vol. 13, no. 12, pp. 6629–6642, Dec. 2014.

[8] K. J. Kim, T. Q. Duong, and H. V. Poor, "Outage probability of single-carrier cooperative spectrum sharing systems with decode-and-forward relaying and selection combining," *IEEE Trans. Wireless Commun.*, vol. 12, no. 2, pp. 806–817, Feb. 2013.

[9] P. Yang, L. Luo, and J. Qin, "Outage performance of cognitive relay networks with interference from primary user," *IEEE Commun. Letters*, vol. 16, no. 10, pp. 1695–1698, 2012.

[10] V. Asghari and S. Aissa, "End-to-end performance of cooperative relaying in spectrum-sharing systems with quality of service requirements," *IEEE Trans. Veh. Technol.*, vol. 60, no. 6, pp. 2656–2668, Jul. 2011.

[11] F. A. Khan, K. Tourki, M. S. Alouini, and K. A. Qaraqe, "Delay performance of a broadcast spectrum sharing network in Nakagami-$m$ fading," *IEEE Trans. Veh. Technol*, vol. 63, no. 3, pp. 1350–1364, Mar. 2014.

[12] T. T. Tran and K. Hyung Yun, "Exploitation of spatial diversity in a novel cooperative spectrum sharing method based on PAM and modified PAM modulation," *Journal of Commun. and Networks*, vol. 16, no. 3, pp. 280–292, June 2014.

[13] ——, "A method to avoid mutual interference in a cooperative spectrum sharing system," *Journal of Commun. and Networks*, vol. 16, no. 2, pp. 110–120, Apr. 2014.

[14] ——, "Exploitation of diversity in cooperative spectrum sharing with the four-way relaying AF transmission," *Wireless Personal Commun.*, vol. 77, pp. 2959–2980, Mar. 2014.

[15] Y. Han, A. Pandharipande, and S. H. Ting, "Cooperative decode-and-forward relaying for secondary spectrum access," *IEEE Trans. Wireless Commun.*, vol. 8, no. 10, pp. 4945–4950, Aug. 2009.

[16] Y. Han, S. H. Ting, and A. Pandharipande, "Cooperative spectrum sharing with distributed secondary user selection," in *Proc. IEEE Int. Conf. Commun. (ICC)*, pp. 1–5, 2010.

[17] Q. Li, S. H. Ting, A. Pandharipande, and Y. Han, "Cognitive spectrum sharing with two-way relaying systems," *IEEE Trans. Veh. Technol.*, vol. 60, no. 3, pp. 1233–1240, Mar. 2011.

[18] Y. Han, T. See Ho, and A. Pandharipande, "Cooperative spectrum sharing protocol with selective relaying system," *IEEE Trans. Commun.*, vol. 60, no. 1, pp. 62–67, Jan. 2012.

[19] L. Yang, M. S. Alouini, and K. Qaraqe, "On the performance of spectrum sharing systems with two-way relaying and multiuser diversity," *IEEE Commun. Letters*, vol. 16, no. 8, pp. 1240–1243, Aug. 2012.

[20] O. Simeone, I. Stanojev, S. Savazzi, Y. Bar-Ness, U. Spagnolini, and R. Pickholtz, "Spectrum leasing to cooperating secondary ad hoc networks," *IEEE J. Select. Areas in Commun.*, vol. 26, no. 1, pp. 203–213, Jan. 2008.

$$F_2(\alpha,\beta,\gamma,\varepsilon)=0,\forall\beta>\gamma, \tag{76}$$

$$\begin{aligned}F_2(\alpha,\beta,\gamma,\varepsilon)&=\int_{\beta}^{\gamma}Q\left(\tfrac{\alpha(\varepsilon+v)\sqrt{2}}{\sigma_{\mathrm{X}}}\right)p_{X_{\dot m}}(v)\,dv=\tfrac{1}{\pi}\int_{0}^{\pi/2}\int_{\beta}^{\gamma}\exp\left(-\tfrac{\alpha^2(\varepsilon+v)^2}{\sigma_{\mathrm{X}}^2\sin^2\theta}\right)p_{X_{\dot m}}(v)\,dv\\&=\varphi(\alpha,\beta,\gamma,\varepsilon),\forall(\beta\le\gamma)\cap(\min\{\alpha(\varepsilon+\beta),\alpha(\varepsilon+\gamma)\}\ge 0),\end{aligned} \tag{77}$$

$$\begin{aligned}F_2(\alpha,\beta,\gamma,\varepsilon)&=\int_{\beta}^{\gamma}Q\left(\tfrac{\alpha(\varepsilon+v)\sqrt{2}}{\sigma_{\mathrm{X}}}\right)p_{X_{\dot m}}(v)\,dv=\int_{\beta}^{\gamma}\left(1-Q\left(-\tfrac{\alpha(\varepsilon+v)\sqrt{2}}{\sigma_{\mathrm{X}}}\right)\right)p_{X_{\dot m}}(v)\,dv\\&=Q\left(\tfrac{\beta\sqrt{2}}{\sigma_{\mathrm{X}}}\right)-Q\left(\tfrac{\gamma\sqrt{2}}{\sigma_{\mathrm{X}}}\right)-\tfrac{1}{\pi}\int_{0}^{\pi/2}\int_{\beta}^{\gamma}\exp\left(-\tfrac{\alpha^2(\varepsilon+v)^2}{\sigma_{\mathrm{X}}^2\sin^2\theta}\right)p_{X_{\dot m}}(v)\,dv\\&=Q\left(\tfrac{\beta\sqrt{2}}{\sigma_{\mathrm{X}}}\right)-Q\left(\tfrac{\gamma\sqrt{2}}{\sigma_{\mathrm{X}}}\right)-\varphi(\alpha,\beta,\gamma,\varepsilon),\forall(\beta\le\gamma)\cap(\max\{\alpha(\varepsilon+\beta),\alpha(\varepsilon+\gamma)\}<0),\end{aligned} \tag{78}$$

$$\begin{aligned}F_2(\alpha,\beta,\gamma,\varepsilon)=&\int_{\beta}^{\gamma}Q\left(\tfrac{\alpha(\varepsilon+v)\sqrt{2}}{\sigma_{\mathrm{X}}}\right)p_{X_{\dot m}}(v)\,dv=\int_{\beta}^{-\varepsilon}\left(1-Q\left(-\tfrac{\alpha(\varepsilon+v)\sqrt{2}}{\sigma_{\mathrm{X}}}\right)\right)p_{X_{\dot m}}(v)\,dv+\int_{-\varepsilon}^{\gamma}Q\left(\tfrac{\alpha(\varepsilon+v)\sqrt{2}}{\sigma_{\mathrm{X}}}\right)p_{X_{\dot m}}(v)\,dv\\=&Q\left(\tfrac{\beta\sqrt{2}}{\sigma_{\mathrm{X}}}\right)-Q\left(\tfrac{-\varepsilon\sqrt{2}}{\sigma_{\mathrm{X}}}\right)-\varphi(\alpha,\beta,-\varepsilon,\varepsilon)+\varphi(\alpha,-\varepsilon,\gamma,\varepsilon),\forall(\beta\le\gamma)\cap(\alpha(\varepsilon+\beta)<0<\alpha(\varepsilon+\gamma)),\end{aligned} \tag{79}$$

$$\begin{aligned}F_2(\alpha,\beta,\gamma,\varepsilon)=Q\left(\tfrac{-\varepsilon\sqrt{2}}{\sigma_{\mathrm{X}}}\right)-Q\left(\tfrac{\gamma\sqrt{2}}{\sigma_{\mathrm{X}}}\right)-\varphi(\alpha,-\varepsilon,\gamma,\varepsilon)+\varphi(\alpha,\beta,-\varepsilon,\varepsilon),\\\forall(\beta\le\gamma)\cap(\alpha(\varepsilon+\gamma)<0<\alpha(\varepsilon+\beta)).\end{aligned} \tag{80}$$


[21] Y. Yan, J. Huang, and J. Wang, "Dynamic bargaining for relay-based cooperative spectrum sharing," *IEEE J. Select. Areas in Commun.*, vol. 31, no. 8, pp. 1480–1493, Aug. 2013.

[22] D. Liu, W. Wang, and W. Guo, "'Green' cooperative spectrum sharing communication," *IEEE Commun. Letters*, vol. 17, no. 3, pp. 459–462, Mar. 2013.

[23] C. Zhai, W. Zhang, and G. Miao, "Cooperative spectrum sharing between cellular and ad-hoc networks," *IEEE Trans. Wireless Commun.*, vol. 13, no. 7, pp. 4025–4037, July 2014.

[24] M. Karaca, K. Khalil, E. Ekici, and O. Ercetin, "Optimal scheduling and power allocation in cooperate-to-join cognitive radio networks," *IEEE/ACM Trans. Networking*, vol. 21, no. 6, pp. 1708–1721, June 2013.

[25] W. Lu, Y. Gong, S. H. Ting, X. L. Wu, and N. T. Zhang, "Cooperative OFDM relaying for opportunistic spectrum sharing: Protocol design and resource allocation," *IEEE Trans. Wireless Commun.*, vol. 11, no. 6, pp. 2126–2135, June 2012.

[26] R. Manna, R. H. Y. Louie, Y. Li, and B. Vucetic, "Cooperative spectrum sharing in cognitive radio networks with multiple antennas," *IEEE Trans. Signal Process.*, vol. 59, no. 11, pp. 5509–5522, Nov. 2011.

[27] W. Lu and J. Wang, "Opportunistic spectrum sharing based on full-duplex cooperative OFDM relaying," *IEEE Commun. Letters*, vol. 18, no. 2, pp. 241–244, Feb. 2014.

[28] X. Feng, G. Sun, S. Gan, F. Yang, X. Tian, X. Wang, and M. Guizani, "Cooperative spectrum sharing in cognitive radio networks: A distributed matching approach," *IEEE Trans. Commun.*, vol. 62, no. 8, pp. 2651–2664, Aug. 2014.

[29] Y. Pei and Y-C. Liang, "Cooperative spectrum sharing with bidirectional secondary transmissions," *IEEE Trans. Veh. Technol.*, vol. 64, no. 1, pp. 108–117, Jan. 2015.

[30] H. Hakim, W. Ajib, and H. Boujemaa, "Spectrum sharing for bidirectional communication exploiting zero-forcing and singular value decomposition beamforming," in *Proc. IEEE Global Commun. Conf.*, pp. 878–883, 2013.

[31] W. Lu, J. Wang, W. Ge, F. Li, J. Hua, and L. Meng, "An anti-interference cooperative spectrum sharing strategy with joint optimization of time and bandwidth," *Journal of Commun. and Networks*, vol. 16, no. 2, pp. 140–145, Apr. 2014.

[32] J. Proakis and M. Salehi, *Digital Communications*, 5th ed., McGraw-Hill, 2008.

[33] A. L. C. Hui and K. B. Letaief, "Successive interference cancellation for multiuser asynchronous DS/CDMA detectors in multipath fading links," *IEEE Trans. Commun.*, vol. 46, no. 3, pp. 384–391, Mar. 1998.

[34] P. Patel and J. Holtzman, "Analysis of a simple successive interference cancellation scheme in a DS/CDMA system," *IEEE J. Select. Areas in Commun.*, vol. 12, no. 5, pp. 796–807, Jun. 1994.